eLife

Reviewed Preprint
v1 • June 18, 2026
Not revised

For correspondence:
lxma@fudan.edu.cn
sujz@wmu.edu.cn
saiyin@fudan.edu.cn

* The authors equally contributed to this work

Competing interests: No competing interests declared

Funding: See page 29

Reviewing editor: Frederic A Bard, Centre de Recherche en Cancérologie de Marseille, France

Fragile polyQ assemblies cause Golgipathy in Huntington's disease

Lixiang Ma[1,*], Xinyu Chen[1,*], Yang Liu[1,*], Lijun Dai[2,*], Fangzhou Ye[1,*], Weiqi Yang[1,*], Hada Buhe[1], Jixin Ma[1], Chenyun Song[1], Li Li[3], Dandan Fan[2], Fanxun Chen[4], Haoman Chen[4], Jianwei Shuai[4], Jianzhong Su[2], Hexige Saiyin[4]

[1]Department of Anatomy, Histology & Embryology, School of Basic Medical Science, Fudan University, Shanghai, China • [2]Department of Anesthesiology, Huashan Hospital, Fudan University, Shanghai, China • [3]Oujiang Laboratory (Zhejiang Lab for Regenerative Medicine, Vision and Brain Health), Wenzhou Medical University, Zhejiang, China • [4]Wenzhou Institute, University of Chinese Academy of Sciences, Wenzhou, China

eLife Assessment

In this study, the authors propose a role for the Huntingtin protein in the organization of the Golgi apparatus and examine the effect of polyQ aggregates at the Golgi. The observations are interesting and potentially **important** for the field; however, the key claim that polyQ HTT functionally disrupts the Golgi (Golgipathy) is **incompletely** supported by the data.

https://doi.org/10.7554/eLife.111495.1.sa3

Abstract

Huntingtin (HTT) is a naturally aggregating protein that causes Huntington's disease (HD) when its polyglutamine (polyQ) tract exceeds 38 repeats. Despite its importance, the biology of HTT aggregates remains poorly defined. Utilizing high-resolution imaging of HD family-derived cells, we have redefined polyQ assemblies—formerly viewed as pathogenic aggregates—as dynamic structures resembling knitted-fabric patches. These assemblies encircle the Golgi apparatus, integrating ribbons and stacks to form a functional polyQ assembly-Golgi complex and attaching clathrin vesicles. Mechanistically, we show that the fragmentation of polyQ assemblies is dynamically coupled with mitotic Golgi fragmentation and that treatment with the ARF inhibitor Brefeldin A splits and fragments the complex. The presence of mutant HTT (mHTT) 'crisps' these assemblies and complexes, altering their response to nutrient deprivation and autophagy enhancers but not to antisense oligonucleotide (ASO) therapy. The polyQ assembly in HD cells also reduces the scaffolding capacity of the Golgi apparatus, clathrin vesicles, and ARF1, impairing Golgi functions. Our results demonstrate that mHTT disrupts the homeostatic dynamics of the polyQ assembly-Golgi complex, inducing a 'Golgipathy' by crippling Golgi structure and function.

Introduction

Huntington's disease (HD) is a devastating neurodegenerative disorder characterized by irreversible neuronal loss in the striatum, resulting in profound motor dysfunction and cognitive decline(Kernich, 2002; Saudou and Humbert, 2016; Walker, 2007a). The condition is driven by the expansion of a polyglutamine (polyQ) tract within the Huntingtin (HTT) protein, rendering it highly prone to aggregation (Gutekunst et al., 1999). Notably, HTT aggregates exhibit significant instability following chemical fixation (Ferrante et al., 1997), a histological challenge that can lead to the misinterpretation of polyQ biology and pathophysiology if standardized protocols are not strictly applied.

While polyQ aggregate formation and the presence of intranuclear inclusion bodies are traditionally considered pathological hallmarks of HD (DiFiglia et al., 1997; Gutekunst et al., 1999), their precise role remains controversial.

Emerging evidence suggests a paradox: some studies indicate that aggregate formation may actually increase single-neuron survival (Arrasate et al., 2004), exerting a protective rather than toxic effect (Kim et al., 1999; Saudou et al., 1998). Conversely, soluble monomeric HTT and its transition into oligomeric species—which precede fibril and inclusion body formation—are the primary drivers of cellular toxicity (Hatters et al., 2013; Jimenez-Sanchez et al., 2017; Lajoie and Snapp, 2010; Legleiter et al., 2010; Mukai et al., 2005; Poirier et al., 2002; Takahashi et al., 2008). These observations suggest that mature HTT aggregates may possess critical biological functions rather than being purely pathogenic.

HTT is a stiff protein composed of multiple α-helical and PolyQ (Dougan et al., 2009; Guo et al., 2018; Saudou and Humbert, 2016; Sivaramakrishnan et al., 2008; Tabrizi et al., 2020). Expanded polyQ (>35) and short polyQ form a rigid fibril (Bauerlein et al., 2017; Dougan et al., 2009; Isas et al., 2017; Scherzinger et al., 1999); however, expanded polyQ fibrils have been reported to physically disrupt organelle membranes, such as the endoplasmic reticulum (ER), and alter membrane dynamics (Bauerlein et al., 2017). Functionally, HTT acts as a versatile scaffold involved in a wide array of cellular processes, including vesicular transport, autophagy, gene transcription, and embryonic development (Saudou and Humbert, 2016). HTTs are an essential protein in embryonic development (Dragatsis et al., 1998; Duyao et al., 1995; Zeitlin et al., 1995). The presence of mutant HTT (mHTT) precipitates widespread cellular dysfunction, ranging from early transcriptional dysregulation and synaptic impairment to mitochondrial distress and disruption of the nuclear pore complex (Costa et al., 2010; del Toro et al., 2009; DiFiglia et al., 1997; Grima et al., 2017; Kim et al., 2010; Mehta et al., 2018; Milnerwood et al., 2006; Saudou and Humbert, 2016; Shirasaki et al., 2012). mHTT induces extrasynaptic excitotoxicity(Milnerwood et al., 2010), higher levels of brain inflammation(Lee et al., 2020; Silvestroni et al., 2009), abnormal fetal brain development(Barnat et al., 2020), and aging(Machiela and Southwell, 2020).

HAP40 stabilizes HTT(Guo et al., 2018; Harding et al., 2021). HTT interacts with and activates dynamin, a protein that catalyzes membrane fission (Caviston et al., 2007; Caviston et al., 2011; Morlot and Roux, 2013), microtubule motors, and actin-associated adaptors to support cellular vesicle transport, including autophagy, endosomes, and lysosomes (Caviston et al., 2011; Olenick and Holzbaur, 2019).

Using HD family-derived cells and super-resolution scanning, we revealed a knitted-fabric-like network formed by HTT polyQ that encircles flat Golgi stacks/cisternae and dynamically couples with both mitotic and stress-related Golgi fragmentation. We demonstrate that while normal polyQ assemblies support the structural integrity of the Golgi, pathogenic mHTT "crisps" these assemblies, destabilizing the complex and impairing Golgi activities. Our findings reveal that the polyQ assembly-Golgi complex is a highly organized functional unit, the disruption of which represents a central mechanism of mHTT-induced toxicity.

Results

Characterization of endogenous polyQ aggregate structure

We identified an HD family in the Mongolian population of West China. 24 persons have identifiable syndromes, including an adult-onset, abnormal gait, uncontrolled arm, leg, and head movements, and psychiatric abnormalities; some patients with severe syndromes showed mania and pica (Table S1). The self-reported symptoms appeared at ages 24 to 50; patients died from 35 to 56 (Table S1). Genetic testing revealed that the patients in this family harbor 44 to 59 CAG repeats in *HTT* (Fig. 1A, B; Table S1), compared with 18-19 CAG repeats in healthy individuals. Consistent with HD, the lengths of CAG repeats define the disease onset age, symptom severity, and death age (Fig. 1C; Table S1).

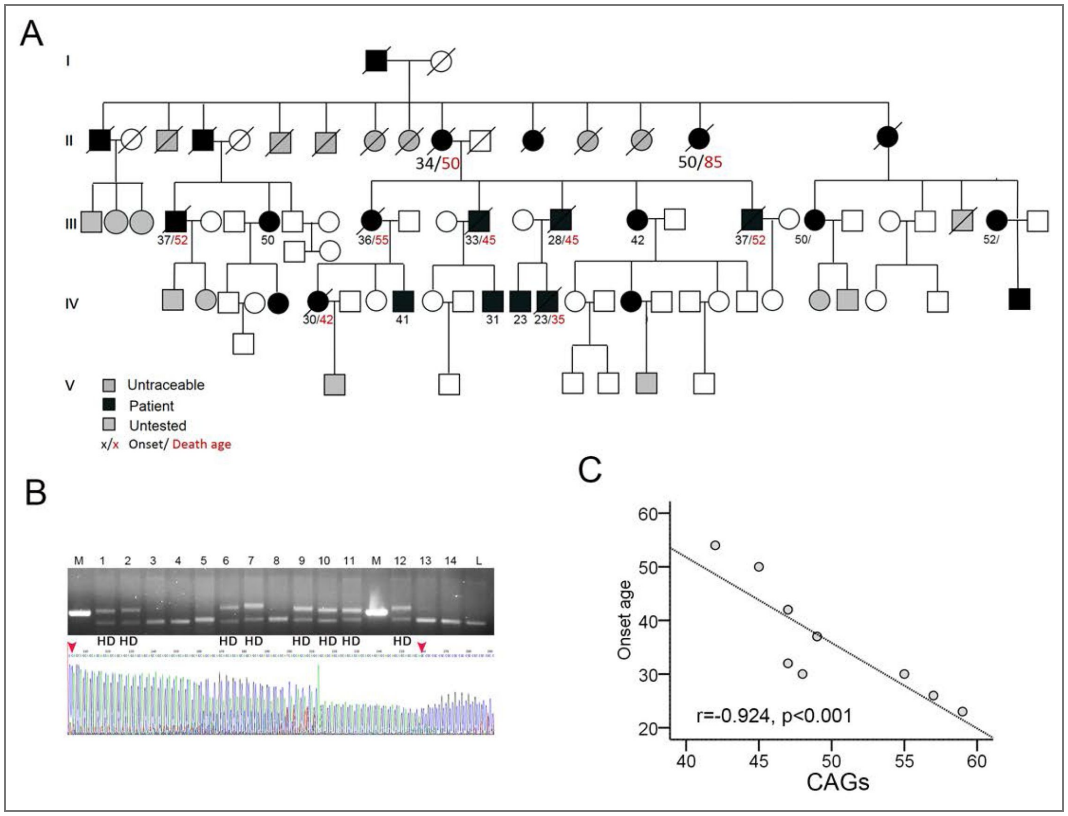

Figure 1. **Identification of a family with HD**

A. The pedigree of the family with HD. **B.** PCR results showed that 8 of 14 are heterogeneous; the upper band is the expanded CAGs (upper panel). Sanger sequencing revealed that the heterogeneous segment contains expanded CAG repeats (lower panel; 49 repeats; red arrows indicate the beginning and end of the CAG repeats). (See also Table S1). M, control band (CAG 35); L, Healthy local person. **C.** The correlations of CAG repeat with disease onset age (Spearman's correlation).

To assess polyQ status in fibroblasts from this HD family, we stained them with the 3B5H10 antibody, a polyQ antibody that equally recognizes both HTT and mHT polyQ (Owens et al., 2015). We observed that the polyQ of fibroblasts, including patients and healthy siblings, exhibits well-organized assemblies that resemble knitted fabrics formed by two paralleled spindles that interfused at a regular interval, structurally resembling an assembly of multiple rings (Fig. 2A). Contrary to other observation(Tousley et al., 2019), phalloidin counterstaining showed that the polyQ assembly did not regularly parallel actin filaments and randomly interact with action filaments (Fig. 2A). 3D rendered tomography showed that the polyQ assembly in fibroblasts interacts with the nuclear membrane (Fig. 2A). Notably, the size of polyQ assemblies in HD is similar to that in healthy fibroblasts (HD: n=4; healthy: n=4) (Fig. 2B, C). Mitochondria did not preferentially enrich in the polyQ assembly site: some of them were present in the polyQ assembly network's space, others were not (Fig. 2D). The polyQ assemblies were fragmented in mitotic cells (Fig. 2E). Strikingly, the polyQ assemblies fragmented after 4% PFA fixation: the immediate staining after fixation is the only way to visualize an intact polyQ assembly (Fig. 2F). These findings indicate that polyQ assemblies are a unique, dynamic polyQ assembly with a specific structure in cells.

PolyQ assemblies of HD patients and healthy individuals differentially respond to stress and drugs

Antisense oligonucleotides (ASOs) reduce the transcription of *HTT(*Kordasiewicz et al., 2012*)*. To test how the polyQ assemblies in fibroblasts respond to ASO, we treated the HD family fibroblasts with ASO (20 and 40 μM) and found that the ASO equally reduced the polyQ assemblies in healthy and HD fibroblasts without affecting the structure of polyQ assembly (Fig. 3A-C). Autophagy-enhancing agents were reported to reduce mHTT(Martin et al., 2015). We also treated HD fibroblasts with onjisaponin F (5, 10, 20, and 40 μM), an active component of the polygala tenuifolia(Nagai et al., 2001). Onjisaponin F reduced polyQ assemblies in HD fibroblasts, but not those in healthy fibroblasts, in a dose-dependent manner, without fragmenting polyQ assemblies (Fig. 3D, E). To see how the polyQ assemblies respond to energy deprivation, we cultured the fibroblasts from 4 patients with HD (CAG: 48, 49, 55, and 59) and 2 healthy siblings in a low-glucose medium. We fixed cells at 24, 48, and 72 h and evaluated the polyQ assemblies. Under glucose deprivation, the polyQ assemblies in HD fibroblasts are diminished and fragmented over time. In contrast, polyQ assemblies in healthy fibroblasts are stable, and the smaller polyQ fragments in healthy cells are decreased (Fig. 3F-H). After culturing in the low-glucose medium for 72 h, we switched to a high-glucose medium. After culturing for an additional 48 h, we observed that the polyQ assemblies in HD fibroblasts had been restored (Fig. 3F-H).

Together, the presence of pathogenic polyQ shifts the response of polyQ assemblies to energy deprivation and to an autophagy-enhancing treatment in fibroblasts.

PolyQ assemblies circle the Golgi apparatus

HTTs are present on the surface of the Golgi, and mHTT impairs Golgi trafficking (del Toro et al., 2009; del Toro et al., 2006; DiFiglia et al., 1995). To our knowledge, the appearance of polyQ assemblies resembles Golgi ribbons. GM130, a Golgi marker, and 3B5H10 coimmunostaining revealed that polyQ assemblies circle flat Golgi ribbon/stacks; the flat Golgi stack stands between the internal space of two parallel spindles of polyQ assemblies, and an isthmus-like hollow in Golgi appeared at where polyQ circled Golgi cisternae (Fig. 4A), indicating the physical interactions of the Golgi apparatus with polyQ assemblies. The size of the Golgi apparatus in HD fibroblasts is smaller than that of healthy cells (Fig. 4B). Clathrin-coated vesicles sort on Golgi(Klumperman, 2011). Clathrin+ vesicles preferentially distributed along or conjugated with polyQ assemblies (Fig. 4C), and polyQ assemblies in HD fibroblasts attached fewer clathrin^{+} vesicles than polyQ assemblies in healthy fibroblasts (Fig. 4D). To localize the C-terminal of HTT in the polyQ assemblies, we stained the polyQ with a 3B5H10 antibody and the C-terminal with a C-terminal-specific antibody (LSB11011) and found that discontinuous C-terminal signals are present in the

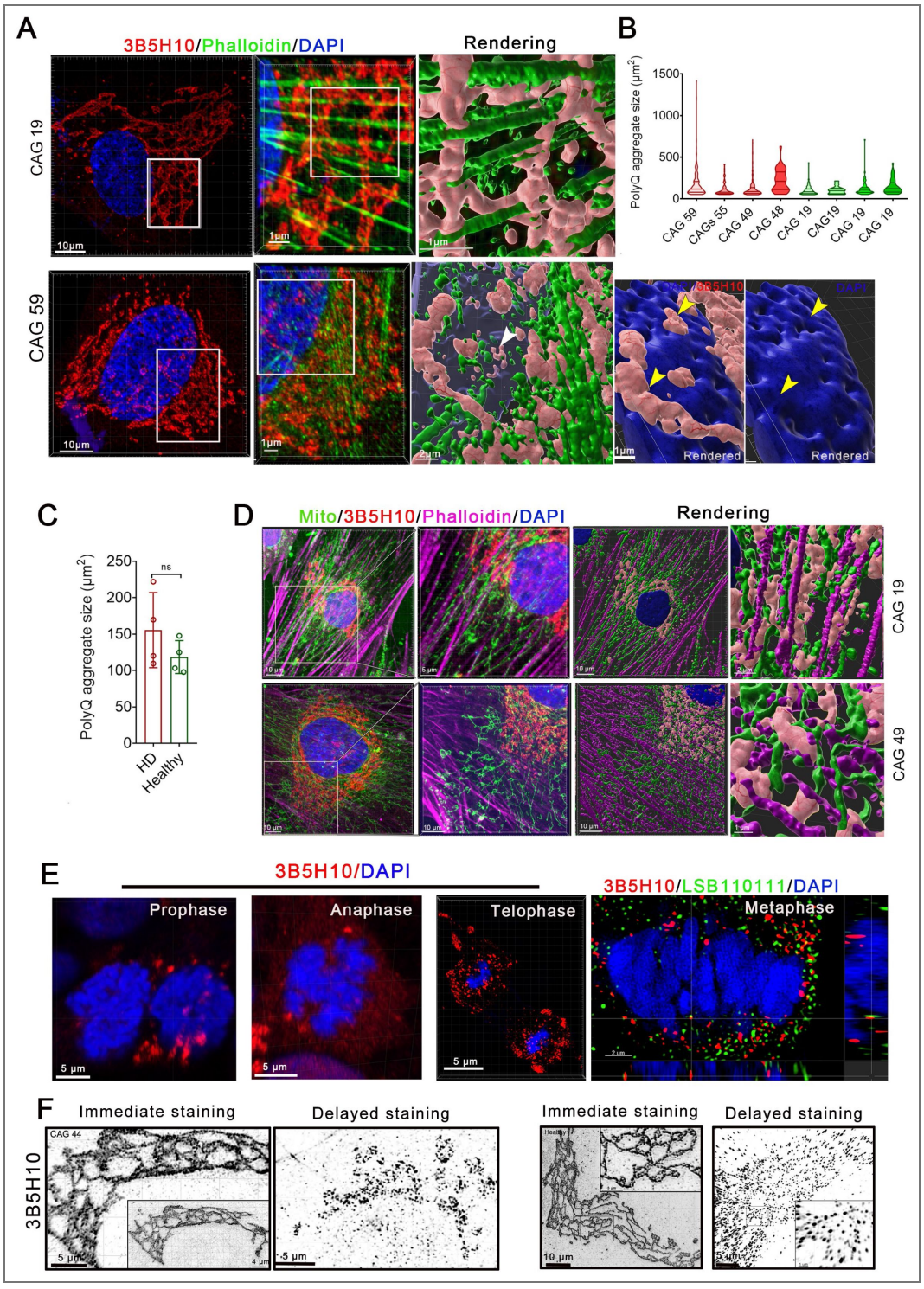

Figure 2. Characteristics of polyQ assembly and polyQ nuclear deposition in neurons

A. DIC images and 3D rendered tomography showing longer polyQ assemblies form a gorge in the cytoplasm or nuclear surface of induced neurons cultured for 75 days (CAG 59 and CAG 19) (pink arrow [i, ii], the gorges; white arrow, nuclear surface dents visualized by IMARIS surface). Inner panels and 3D rendered tomography displayed the spatial relationships. **B.** PolyQ deposits into the nucleus and pokes the nuclear membrane of striatal neurons (white arrow, the morphology of the nucleus; yellow arrows, nucleus poked by polyQ assemblies). The lower left in right panel is an apoptotic cell (CAG, 55). **C.** PolyQ precipitates occupied the nucleus of GABAergic neurons cultured for 178 days (CAG, 47). **D, E.** HD patient striatal neurons derived from iPSCs cultured for 90 days (2D culture) (CAG 59) and 98 days (CAG 55) and 110 days (CAG 47) have spliced nucleus (white arrows, spliced nucleus). The summary table of nuclear splicing.

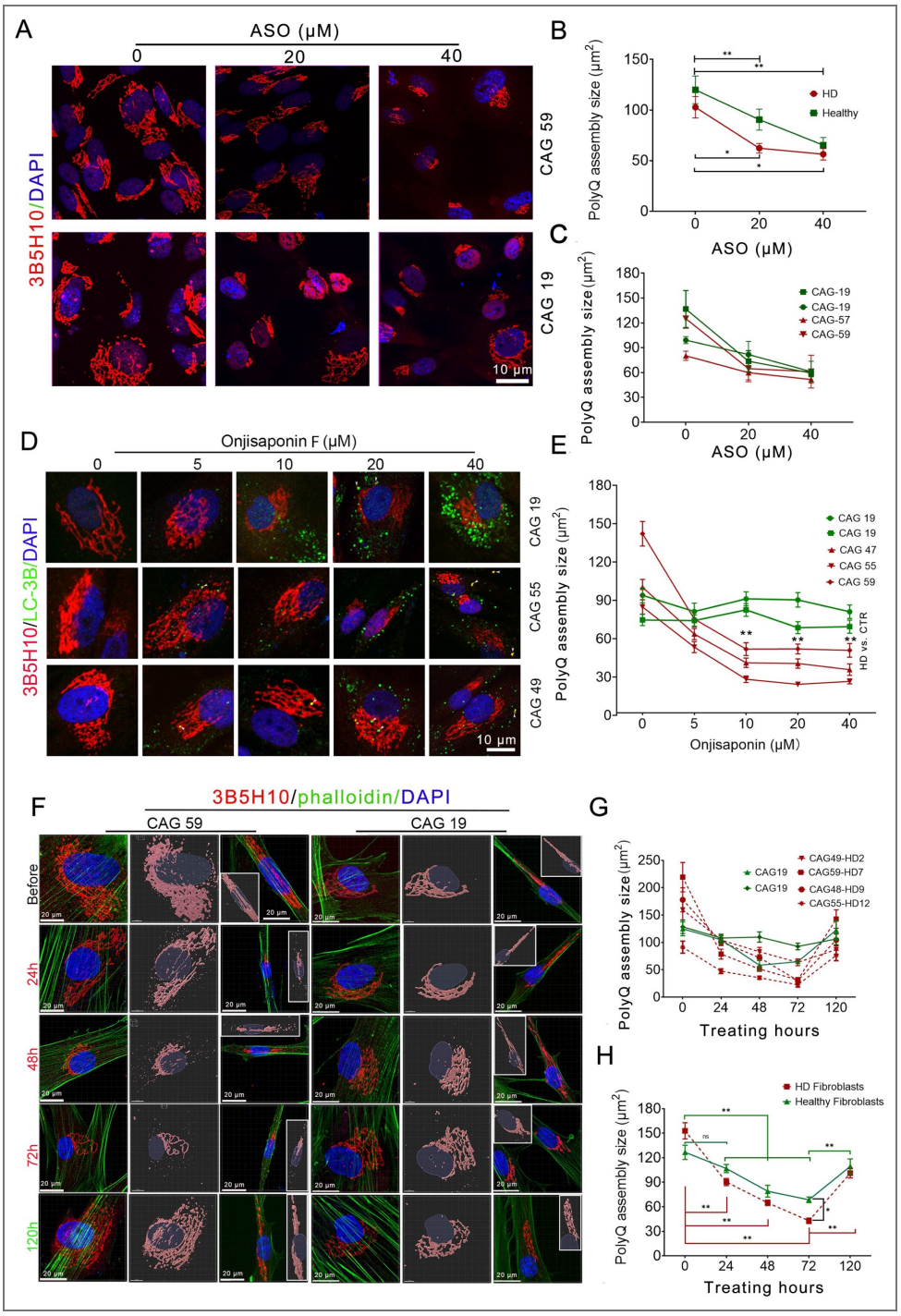

Figure 3. PolyQ assemblies of HD and healthy individuals differentially respond to stress and drugs

A. The representative polyQ assemblies in ASO-treated HD and healthy fibroblasts stained by the 3B5H10 antibody. **B, C.** The changes in polyQ assembly size in ASO treatments. Comparing the trends of changes in HD with healthy (B); The changes of polyQ assembly in each individual (C) (HD, n=2 [CAG 57 and 59]; Healthy, n=2; Two-way ANOVA, * <0.05; **<0.01). **D.** The immunostaining of Onjisaponin F-treated HD and healthy fibroblasts with LC-3B and 3B5H10 antibody. **E.** The changes in polyQ assembly size in Onjisaponin F treatments. The trends of changes in HD and healthy individuals (HD, n=3; Healthy, n=2; Two-way ANOVA, **<0.01). **F.** 3B5H10 stained polyQ assemblies under glucose starvation in the HD and healthy fibroblasts at different time points. The middle panels and the inserted image (second panel) are 3D rendering tomography in IMARIS. **G, H.** The size changes of polyQ assemblies under glucose starvation in the fibroblasts of healthy siblings and HD patients at different time points. The change of polyQ assembly in the fibroblast of each individual (G) (Red line, HD patients; Green line, healthy), comparing the change of polyQ in HD with healthy (H) (Two-way ANOVA, **<0.01).

polyQ assemblies, and the C-terminal of HCC reside inside the assembly (Fig. 4E). We also noticed that some smaller polyQ assemblies which conjugate with abundant actin filiaments are present in the cytoplasm or ruffluring membrane of fibroblasts (Fig.S1A-C).

Huntingtin-associated protein 40 (HAP40), a protein coevolved with HTT, binds to all three domains of HTT and stabilizes HTT(Guo et al., 2018; Harding et al., 2021). HAP40 resided on the corner of the network in polyQ assemblies, polyQ assemblies in HD, and healthy cells attached the same amount of HAP40 (Fig. 4F, G).

The Golgi apparatus fragments during cell mitosis and reassembles after mitosis (Wei and Seemann, 2009). PolyQ assemblies and Golgi stack/ribbon fragment during prometaphase (28 cells from 6 samples) and anaphase (23 cells from 6 samples), and reassemble at the late telophase (22 cells from 6 samples), and the fragmented Golgi in the mitotic cells conjugate with polyQ patches (Fig. 4H). Consistent with our previous reports(Liu et al., 2024), the polyQ assemblies in HD fibroblasts attached fewer ARF1, and Brefeldin A (BFA) treatments decouple polyQ assemblies from the Golgi apparatus in all fibroblasts (Fig. 4I-M). ARF1, which conjugates to the Golgi after converting its GDP to GTP-ATP in a GTP-ATP-dependent manner(D'Souza-Schorey and Chavrier, 2006), couples polyQ assembly to the Golgi (Liu et al., 2024). Thus, it is rational to hypothesize that polyQ assembly in HD fibroblasts is sensitive to energy deprivation. To test this hypothesis, we also immunostained HD patient fibroblasts and their healthy siblings that had been starved for 48 h with antibodies against 3B5H10 and GM130. Consistent with the changes of polyQ assemblies of HD and healthy cells under stress, the Golgi ribbons of HD fibroblasts loosened and fragmented, and most polyQ fragments/patches attached by Golgi fragments in glucose deprivation (Fig. S1F), whereas the structure of Golgi ribbons is stable, and the small Golgi fragments are reduced in healthy fibroblasts after culturing in a low glucose medium for 48h (Fig. S1F, G). In addition, we observed that HD patient cells with higher CAG repeat counts (55) had more fragmented Golgi than those with lower CAG repeat counts (49) after 48 h of glucose deprivation (Fig. S1H). The size of the Golgi in HD fibroblasts is reduced more quickly than that of its healthy siblings after 48 h glucose starvation (Fig. S1I). Together, our findings indicate that polyQ assemblies form a polyQ assembly-Golgi apparatus complex impaired by the presence of mHTT. To see *in vivo* Golgi dynamics in a living fibroblast, we continuously monitored fibroblasts (CAG: 49, 55, 19, and 19) stained by Golgi apparatus-selective dye after glucose starvation or H2O2 stimulation. The Golgi apparatus in HD patient fibroblasts is easier to fragment under glucose starvation than healthy fibroblasts (Fig. 4N, O), whereas the Golgi apparatus in patients and healthy fibroblasts uniformly fragments under H202 stimulation (Fig. S1D, E).

Impaired polyQ assembly in HD neurons is associated with deficient golgi function in cortical and striatal neurons

We generated iPSCs from the family fibroblasts and differentiated them into GABAergic projection neurons in 2D (Ma et al., 2012). On day 90, long polyQ assemblies are present in striatal neuronal projections, and fragmented polyQ assemblies were deposited in the neuronal nucleus of an HD patient with CAG 59 (Fig. 5A). PolyQ almost completely occupied the nucleus of some HD striatal neurons around 100 days in all patient neurons (CAG 47-59), but PolyQ did not appear in the nucleus of healthy striatal neurons with over 90 days of culture (Fig. 5A, B). DIC images revealed that an intact, observable, deeply invaginated gorge where polyQ assemblies reside or traverse appeared in neurons, and 3D tomographic rendering showed that polyQ spindles also created a gorge on the nuclear surface (Fig. S2A), indicating that polyQ assemblies are an intact and rigid structure. In addition, the striatal neurons with polyQ nuclear accumulation showed a pale-stained nucleus, nuclear membranes pocked by polyQ, and nuclear fragmentations (Fig. S2B-F). The fragmentation of polyQ also existed in human fetal and child brain samples, but not in fresh human brain organoid samples (Fig. S3A-C). Despite the fragmentation of polyQ assemblies in brain tissues, the structure of polyQ assemblies and their interaction pattern with the nucleus are identical to those of the polyQ assemblies in human brain organoids (Fig. S3B; Fig.5A, B). The necrosis-dependent fragmentation of polyQ assemblies in brain organoids was common (Fig. S3D). The proteomic data also showed that nuclear activities in the HD striatal organoids

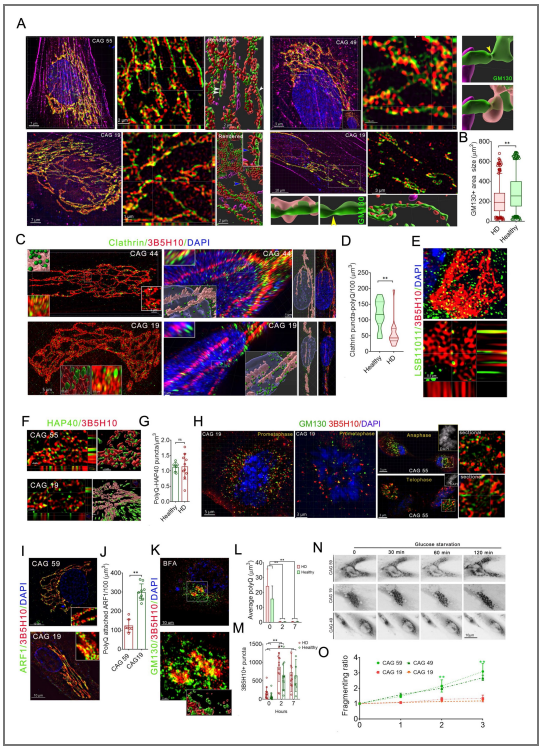

Figure 4. PolyQ assemblies circle the large Golgi apparatus

A. GM130 and 3B5H10 antibodies and phalloidin staining in healthy sibling and HD fibroblasts showed that polyQ assemblies circle the Golgi apparatus (z-stack intervals, 0.2μm). The rendering tomography of Z-stacked images revealed the spatial relationship of polyQ assemblies with the Golgi stack; polyQ assemblies circle the Golgi stack, and a narrowing of GM130-stained Golgi exists in the site where polyQ encircles the Golgi (yellow arrows, isthmus; blue arrows, the arm of polyQ; the boxed region, the magnified part in the right panel). **B.** The size of the GM130-stained Golgi apparatus in HD and healthy individuals (HD, n=3; Healthy, n=3. Student *t*-test; **<0.01). **C.** The representative images of clathrin and 3B5H10 antibody immunostaining in the fibroblasts of an HD patient and healthy fibroblasts. The left is a large polyQ assembly. The inner inserts on the left show angled and rendered views of the spatial relationship between the polyQ assembly and clathrin+ puncta. The right is the interacting pattern of polyQ with the nucleus and attaching patterns of clathrin to polyQ assemblies that interact with the nucleus (inner inserts, rendered view [lower] and the conjugation pattern of clathrin with polyQ assembly [upper]). **D.** The number of Clathrin^{+} vesicles overlapped with polyQ assemblies. The object-object statistics in IMARIS were used to measure overlapping. HD, n=3; Healthy, n=3. Data, mean± SD. Student *t*-test; *<0.05. **E.** HTT C-terminal antibody and polyQ antibody immunostaining revealed that C-terminal antibody signals colocalize with cytoplasmic polyQ assemblies. **F.** Coimmunostaining of 3B5H10 antibody with HAP40 antibody revealed that polyQ assemblies were attached by HAP40. The lefts are sectional views, and the rights are 3D renderings of the middle panel by IMARIS surface. **G.** The count of HAP40 puncta attached to polyQ assemblies in healthy and HD fibroblasts. The distances between HAP40 puncta and polyQ assemblies were measured by IMARIS. HD, n=2; Healthy, n=2. Student t-test; Data, mean ± SD. Student t-test; ns, p>0.05 **H.** The 3B5H10 and GM130 antibodies immunostaining images in the mitotic fibroblasts, including prometaphase, anaphase, and telophase, were obtained by SIM microscopy. The inserted DAPI images (gray) showed the nuclear chromatin structure. The right panels are a sectional view of the boxed region (anaphase and telophase). **I.** ARF1 and 3B5H10 antibody immunostaining in the fibroblasts revealed that ARF1 preferentially interacts with polyQ assemblies. **J.** The measurement of polyQ assembly-conjugated AFR1 puncta in the healthy and HD fibroblasts. Student t-test; **<0.001 **K.** GM130 and 3B5H10 antibody immunostaining in BFA-treated fibroblasts revealed that most fragmented Golgi liberate from polyQ. The boxed region in the upper panel is the magnified region. The lower insert is a 3D rendering of a tomographic image. **L.** The volume of polyQ assemblies/puncta in fibroblasts after 2 hours and 7 hours of treatment by BFA. The measurements were performed using IMARIS software. (Images, n: 7-12. Sample size: n=2 in each group. One-way ANOVA, **<0.01). **M.** The count of 3B5H10-stained assemblies/puncta in the fibroblasts (Images, n: 7-11. Sample size: n=2 in each group. One-way ANOVA, **<0.01). **N.** Image sequences of Golgi labelled by GOLGI ID Green assay kit in the living fibroblasts of healthy siblings and HD patients (CAG 59, 49, and CAG 49) after glucose starvation (The displays, the inverted channel of the original image). **O.** The fragmentation ratio of the Golgi under glucose starvation at different time points in healthy and HD fibroblasts. Fragmentation ratio = number of Golgi of a cell at each time point/ number of Golgi at 0 min (Two-way ANOVA. **<0.01. The number of images in the cell line: n>5).

(hStrO), including chromatin and DNA complex assembly, protein-DNA complex, DNA packaging complex, and nucleosome binding, were impaired in hStrO cultured for more than 60 days (Fig. S4A, B).

We also characterized the relationship between polyQ assemblies and the Golgi in neurons of hStrO and cortical organoids (hCOs) (Fig. S4A, C) (Chen et al., 2022). PolyQ assemblies include a flat Golgi stacks in hCOs, and the surface of Golgi in HD neurons were irregular (Fig. 5C). Multiple Golgi also resided in the polyQ assemblies of striatal neurons in hStrO, which traversed through the nuclear surface (Fig. 5D). PolyQ assemblies in the HD striatal neurons conjugate fewer Golgi than polyQ assemblies in healthy striatal neurons of hStrO (Fig. 5E). Clathrin+ vesicles preferentially distributed along or conjugated to polyQ assemblies in the HD and healthy neurons (Fig. 5F). Consistent with the results of fibroblasts, polyQ assemblies in HD neurons of hStrO attached fewer clathrin+ vesicles and ARF1 than that of healthy polyQ assemblies (Fig. 5F, G; Fig. S5A-C), and Golgi apparatus in HD neurons also attached fewer ARF1 puncta than that of healthy Golgi (Fig. S5D-F). In addition, *ARF1* transcription levels in HD hStrOs are uniformly lower than those of healthy hStrO (60 and 80 days) Fig.S5G, H). Striatal projection neurons have extremely long dendrites and axon(Lanciego et al., 2012).

Extended polyQ assemblies in HD striatal neuronal projections in hStrO, which resemble human striatal neuronal polyQ assembly, attached fewer fragmented/small Golgi than healthy polyQ assemblies (Fig. 5H-I); small Golgi resided in the hole of rings or attached to the outer spines of long polyQ assemblies in hStrO neurons (Fig. 5N). Clathrin+ vesicles interact with the polyQ assemblies and mainly reside on the two sides of the assemblies in the neurons of hStrO (Fig. 5O).

To test the functional impact of deficient polyQ assemblies-Golgi complexes on HD neuronal activities, we performed HD-MEA recordings on 80-day hCOs. Control organoids exhibited robust, highly synchronized network bursts, resembling the coded activity patterns of developing human brains (Fig. 5K). In contrast, HD hCOs displayed erratic firing patterns (Fig. 5K).

Quantitative analysis revealed a significant reduction in both spikes per burst and the inter-burst interval (IBI) in HD hCOs (Fig. 5L). Notably, the elevated IBI CV in HD hCOs signifies a disruption in the periodicity and rhythmic regularity of spontaneous network-wide bursting. These findings demonstrate that polyQ assemblies-mediated pathologenesis disrupts the emergence of functional network oscillations and collective neuronal firing in cortical circuits.

Impaired Golgi function in HD striatal neurons

We performed single-cell RNA sequencing (scRNA-seq) analyses of human striatal organoids (hStrOs) derived from hESC-H9, hiPSC-8-12 (CAG 19), and HD hiPSC-7-2 (CAG 59) after 110 days of culture. Transcriptomic data of 38,716 single cells were obtained after quality control and filtering (Fig. 6A). Uniform manifold approximation and projection (UMAP) clustering identified four clusters in hStrOs that expressed cell-type-specific markers, including progenitor (VIM, NES, HES1), neuron (SYT1, DCX, STMN2), astrocytes (S100β, GFAP), and oligodendrocytes (OLIG2, SOX10) (Fig. 6B, C, and S6A). We further plotted the expression of brain region-specific markers in these clusters and found that both control and HD hStrOs are primarily composed of LGE progenitors and GABAergic neurons rather than cortical progenitors and glutaminergic neurons (Fig. S6C, D), consistent with our protocols for generating hStrOs(Chen et al., 2022). Based on the characteristics of Golgi in HD fibroblasts, we compared the transcriptomes of mature GABAergic neurons in the control and HD groups after sorting the GABAergic neuron population using GAD1 and GAD2, specific markers for mature GABAergic neurons (Fig. S6D-F). In the GABAergic neurons, the DEGs of HD hStrO extensively overlapped with those of hiPSC-derived hStrO (CAG 19) and hESC-derived hStrO, both for up-regulated (321 genes) and down-regulated genes (550 genes) (Fig. 6D). Up-regulated genes in GO terms are associated with nuclear activities, including ribonucleoprotein complex assembly, translational initiation, and regulation of translation, which might be related to the nuclear poking of polyQ assemblies or deposition of polyQ into the nucleus. Interestingly, the down-regulated genes in GABAergic neurons of HD hStrOs were notably enriched for GO terms associated with Golgi or Golgi-related functions,

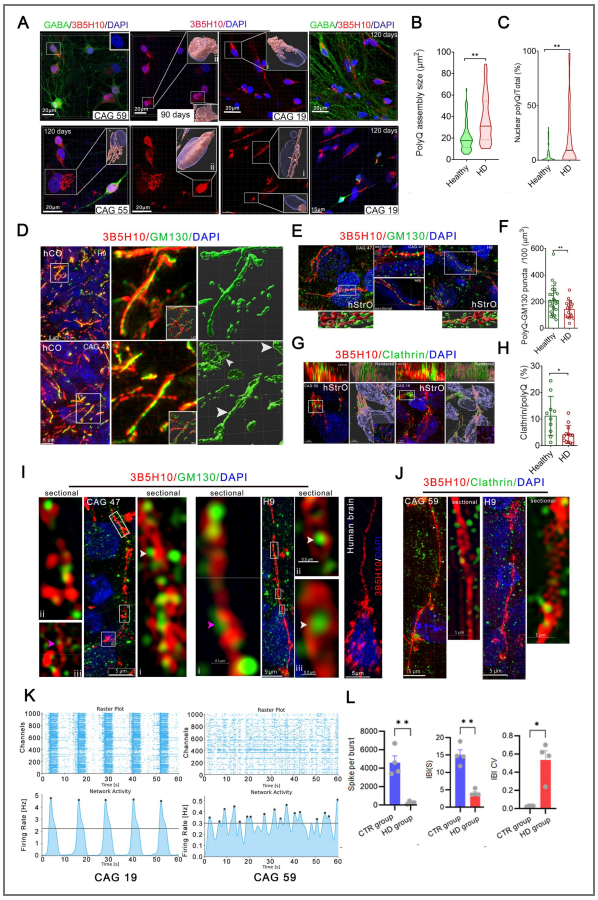

Fig. 5. The characteristics of polyQ assembly in the induced striatal and cortical neurons

A. The characteristics of polyQ assembly in iPS -derived striatal GABAergic neurons at day 90 and 120 (i, the nucleus without nuclear accumulation; ii, the nucleus with nuclear polyQ accumulation). The inner inserts show the 3D tomographic rendering, which revealed the spatial relationship between polyQassemblies and the nucleus. **B.** The size of polyQ assemblies in iPSCs-derived GABAergic neurons (HD, n=4 [CAG 59, 55, 49, and 47]; Healthy, n=3 [CAG 19, CAG 19, and H9]). Data, mean ± SD. t-test; **<0.01. **C.** The percentage of nuclear polyQ volume/total polyQ volume in iPS-derived GABAergic neuronal nucleus cultured over 90 days (HD, n=4 [CAG 59, 55, 49, and 47]; Healthy, n=3 [CAG 19, CAG 19, and H9]). *t*-test; **<0.01. **D.** The representative images of polyQ assemblies and Golgi stained by 3B5H10 and GM130 antibodies in hCO (Taken by SIM microscopy; Z-stack interval, 0.2μm). The right panels show the rendered tomography of the Golgi by Imaris 9.8 surface (white arrows indicate the Golgi with an irregular surface). **E.** The representative images of polyQ assemblies and Golgi stained by 3B5H10 and GM130 antibodies in hStrO (taken by SIM microscopy; Z-stack interval, 0.2 μm). The middle panels are a sectional view of the rectangle. The lower panels are 3D rendering tomography by Imaris 9.8 surface. **F.** Comparing the overlapped volume of the Golgi with polyQ assemblies in HD striatal neurons with that of healthy striatal neurons. The object-object statistic function in Imaris 9.8 measures the overlapped volume (Student *t*-test; **, p <0.01. HD hStrO: CAG 55 and CAG 47; Healthy hStrO: H9, CAG 19. Student *t*-test, *<0.05). **G.** The images of polyQ assemblies stained by 3B5H10 and clathrin antibodies in hStrOs were taken by SIM microscopy (The upper panel, the lateral view of the boxed region; the inner insert in the rendered image, a larger view of the original image). The renderings are done by Imaris surface. **H.** Comparing clathrin+ vesicle volume overlapped with 3B5H10-stained polyQ assemblies of striatal neurons in the healthy sibling with an HD patient. *t*-test, *, p<0.05. HD hStrO: CAG 55 and CAG 47; Healthy hStrO: H9, CAG 19. Student *t*-test; * <0.05. **I.** 3B5H10 and GM130 antibodies immunostaining images and their sectional views in the neurons of hStrO of HD patients and healthy siblings revealed the spatial relationships between polyQ assemblies and Golgi (white arrows, the Golgi in the inner hole of the ring; pink arrows, the scaffolding Golgi; the boxed region, the right or left panel). The right panel is a 3B5H10-stained assembly in a human striatal neuron with a long projection. **J.** 3B5H10 and clathrin antibodies staining images of the neurons in hStrO of HD patients and healthy siblings revealed the spatial relationships between polyQ assemblies and clathrin-stained vesicles. The left panel is a sectional view between two arrows (hStrO at day 80; two white arrows, the segment in the right panel) **K.** The raster plots and network activity of the cortical neurons in HD and healthy hCOs. **L.** Quantification of network features at the burst level in HD and healthy hCOs, including the number of spikes per burst, the interburst intervals (IBI), and IBI CV (CTR group: n=3 hCOs; HD group: n=3 hCOs; The mean ± SD, Welch's t-test, * < 0.05; ** < 0.01).

including Golgi vesicle transport, endoplasmic reticulum to Golgi vesicle–mediated transport, vesicle organization, endomembrane system organization, intracellular protein transport, protein localization to membrane translation (Fig. 6E). The down-regulated genes in HD hStrOs belong to Golgi matrix proteins, including *GOLGA8A*, a structurally similar protein of GM130 enriched in neurons, *GOLGA4*, and Golgi matrix-associated GTPs that include *RAB6*, *ARL1/4C*, and *ARF1/3/4*.

Onjisaponin F did not mitigate polyQ nuclear accumulation, nor did ASO treatment normalize HD neuronal firing rates

We selected iPSCs from two HD patients (CAG 59 and 49), one healthy sibling, and the H9 cell line, and differentiated them into striatal neurons in 2D to test the effects of onjisaponin F on striatal neurons. We exposed iPSC-derived GABAergic neurons to a single dose of 20 μM onjisaponin F for 24 h on days 42 and 60. After culturing for another 48 h, we fixed the striatal neurons, assessed polyQ changes, and found that onjisaponin F treatment on days 42 and 60 reduced polyQ assembly volume in HD striatal neurons but not in healthy neurons (Fig. 7A-C). We treated induced HD and healthy striatal neurons with 3 doses of onjisaponin F for 24h on days 50, 60, and 70. The immunostaining at day 90 showed that 3 doses of onjisaponin (10 μM) decreased the cytoplasmic and total volume of polyQ assemblies in HD striatal neurons but did not reduce the nuclear deposition of polyQ; the immunostaining at day 110 revealed that 3 doses of onjisaponin (20 μM) did not change the volume of polyQ assembly in healthy striatal neurons (Fig.7D-E).

Given that ASOs have demonstrated efficacy in promoting mHTT degradation across experimental models(Kordasiewicz et al., 2012) and have reduced the polyQ assembly size in human fibroblasts. We utilized ASO as a benchmark to evaluate its therapeutic impact on the polyQ assembly-driven phenotypes in hCOs. Following treatment, we observed downward trends in both spikes per burst and the IBI (Fig. 7F, G). The IBI coefficient of variation (CV) also trended lower, suggesting a subtle shift toward improved firing patterns (Fig. 7F, G). However, these alterations failed to reach statistical significance across 10 days (Fig. 7F, G). The analysis of polyQ, Golgi, and ARF1 by immunostaining revealed that ASO treatment reduced the size of polyQ assemblies in HD-hCOs but did not alter the Golgi tomography and inclusion, Golgi/ARF1 conjugation to polyQ assemblies (Fig. 7H-K; Fig. S7A-D). These findings demonstrate that, under the tested conditions, the ASO treatment was insufficient to achieve a significant functional recovery of the HD-hCO network dynamics and rescue the Golgipathy in HD-hCOs.

Discussion

Here, we redefine the biology and structure of HTT polyQ aggregates, previously characterized as pathogenic aggregates(Truant et al., 2008). Using cells from a large, isolated HD family and state-of-the-art scanning, we show the polyQ assemblies of HTTs are large, dynamic, and well-organized structural networks composed of two or more long, parallel, and interfused spindles that encircle the Golgi apparatus, bind clathrin vesicles, and form a polyQ assembly-Golgi complex, which is structurally and dynamically coupled. The presence of mHTT shifts the response of polyQ assembly to energy deprivation and to autophagy-enhancing drugs, and destabilizes the Golgi apparatus by impairing ARF recruitment, inducing a Golgipathy in HD patients.

The Golgi ribbon comprises up to 100 flat stacks, composed of 4-11 stapled cisternae, in which newly synthesized soluble cargo proteins and lipids are processed and sorted, linked by tubular bridges in mammalian cells (Klumperman, 2011; Liu et al., 2021). The Golgi matrix, a ribosome-free protein network surrounding the cisternae, supports the stack structure(Ravichandran et al., 2020). The spatiotemporal relationships of polyQ assemblies with the Golgi apparatus, clathrin-coated vesicles, and ARF1 indicate that rigid polyQ assemblies serve as a structural component of the Golgi matrix, providing a scaffold for the Golgi apparatus and Golgi activities, including shaping, assembly, and sorting. ARFIP2, which interacts or conjugates multiple guanine nucleotide exchange factors (GEFs), including ARF1, ARF3, ARF5, and ARF6 (Wu and Zhou, 2009), directly conjugates with HTTs (Peters et al., 2002). Thus, it is rational to

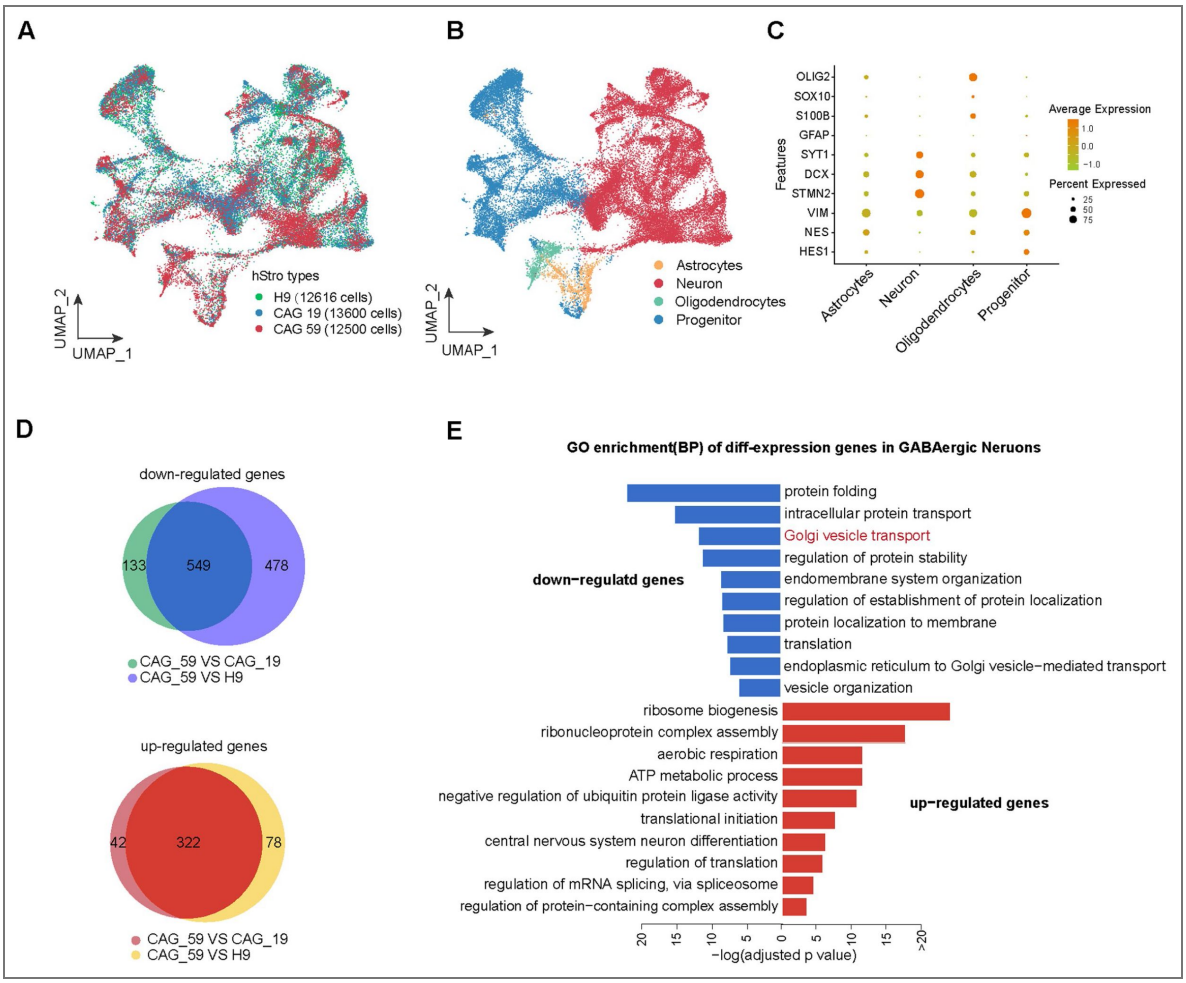

Fig. 6. GABAergic neurons from HD patients reduced Golgi- or vesicle-related activities and intensified nucleus-related activities

A, B. Uniform manifold approximation and projection (UMAP) plot of all cells colored by their sample origin (A) and by cell types(B). C. Dot plot displaying an expression of example marker genes. D. Venn diagram summarizing the number of overlapped genes differentially expressed in CAG59 vs. CAG19/H9 GABAergic neurons. E. GO enrichment analysis of down-regulated (top) and up-regulated (bottom) genes in CAG59 vs. CAG19/H9 GABAergic neurons.

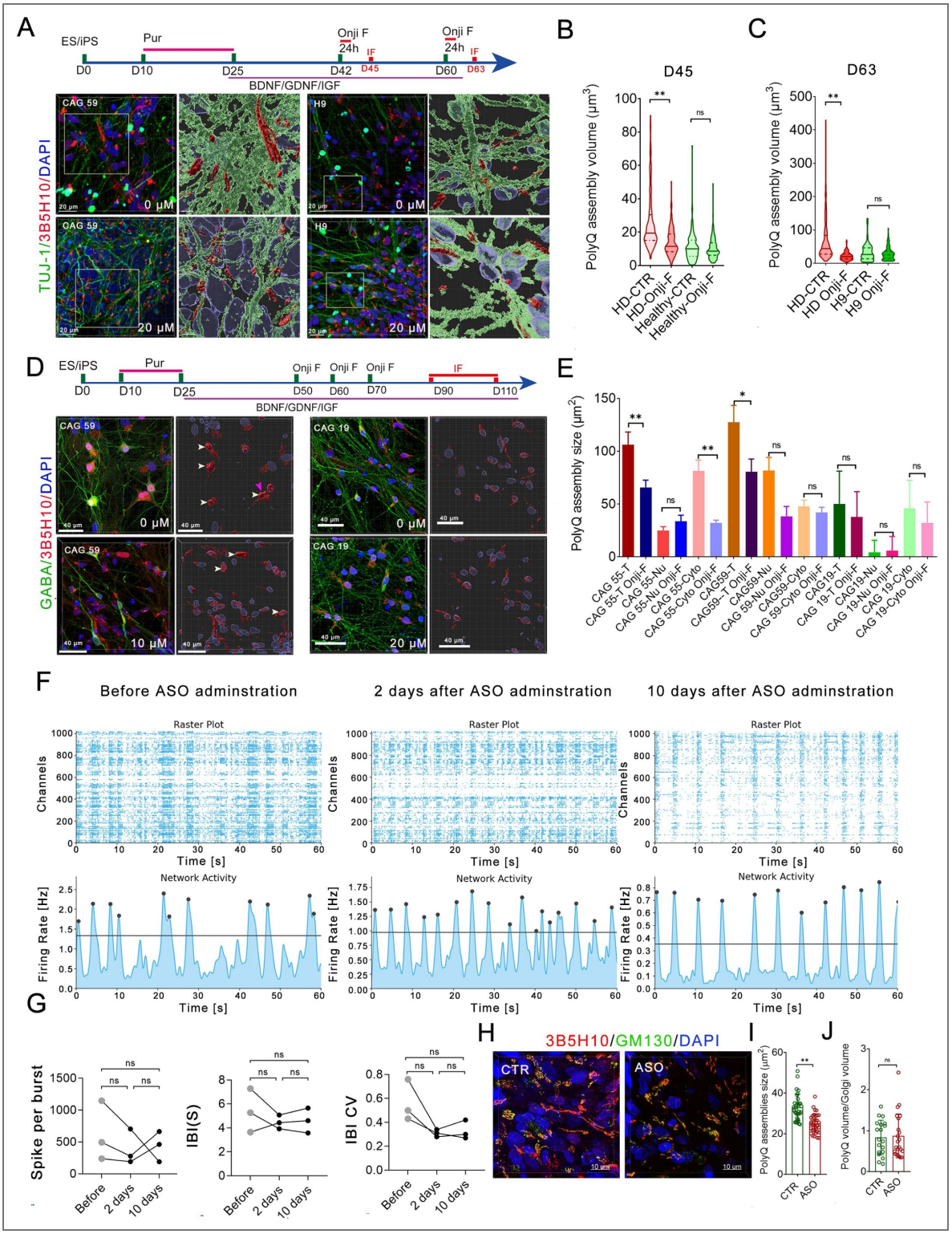

Figure 7. Onjisaponin F did not mitigate polyQ nuclear accumulation, and ASO corrected the aberrant HD striatal neuronal firing

A. The schematics of treatment (upper) and the representative images of polyQ assemblies stained by 3B5H10 antibodies in HD and healthy striatal neurons at 63 days treated by one dose of 20 μM onjisaponin F for 72 h.

hypothesize that the ARFIP2-ARF complex mediates the relationship between polyQ assembly and the Golgi apparatus. The decoupling of the polyQ assembly-Golgi complex by BFA, but not during mitotic Golgi fragmentation, supports that the ARFIP2-ARF1 complex mediates this assembly.

Golgipathy, including structural and functional abnormality, is common in neurodegenerative diseases (El Ghouzzi and Boncompain, 2022; Klumperman, 2011; Liu et al., 2021; Passemard et al., 2017). The correct Golgi positioning is critical for cellular polarization and differentiation (Yadav and Linstedt, 2011); The precise localization of the Golgi apparatus mediates the simple spindle-like cells to form the dentate granule cells (DGCs) (Rao et al., 2018); GM130 deletion causes neurodegeneration and ataxia (Liu et al., 2017).

Pathogenic *GORASP1 and ARF3* variants cause a neurodevelopmental disorder with neurosensory, neuromuscular, and skeletal abnormalities via affecting the cell cycle and glycosylation (Fasano et al., 2022; Lebon et al., 2025; Sakamoto et al., 2021). Previously, we reported that polyQ assemblies in HD cortical neurons altered corticogenesis by impairing ARF1 recruitment to the Golgi apparatus in the neuroepithelium(Liu et al., 2024).

The striatal projection neurons, which contain a prominent long polyQ assembly and polyQ nuclear accumulation, are lost early in HD patients (Walker, 2007b). HTT is a rigid protein (Dougan et al., 2009; Guo et al., 2018; Saudou and Humbert, 2016; Sivaramakrishnan et al., 2008; Tabrizi et al., 2020). The conjugation of ARF1 to the Golgi consumes ATP(D'Souza-Schorey and Chavrier, 2006). The glucose metabolism in HD patients is stronger than that of a healthy individual (Tang et al., 2013). Based on the body's compensation mechanism, the deficient ARF1 conjugation to the Golgi apparatus in HD might contribute to increased brain metabolism. The polyQ assembly-Golgi apparatus complex in HD striatal neurons needs more ATP to stabilize and function. Onjisaponin F, a strong autophagy enhancer, preferentially reduces the polyQ assembly in HD fibroblasts and striatal projection neurons without changing the structure of polyQ assembly. However, it did not rescue nuclear polyQ deposition, a hallmark of HD pathology(DiFiglia et al., 1997). Based on the spatial relationship of polyQ assembly with the neuronal nucleus and the rigid nature of polyQ, it is rational to consider that the fragility of HTT assembly, rather than the size of polyQ assembly, might be the cause of nuclear accumulation in long-term cultured striatal neurons. A well-test ASO(Kordasiewicz et al., 2012) reduced the size of polyQ assemblies in HD cells but did not correct aberrant neuronal firings in HD cortical neurons, indicating that the structure of polyQ assembly-Golgi complex in HD cells drives aberrant neuronal activity. However, the size of polyQ assemblies does not matter.

Our study reveals the structure of polyQ aggregates and their spatial-temporal relationship with the Golgi apparatus, and demonstrates that mHTT destabilizes the polyQ assembly-Golgi complexes, dismantles the recruitment of Golgi activity-related proteins, leading to Golgipathy in HD. Thus, improving Golgi function and stabilizing polyQ assembly in HD might represent another approach to treating HD.

The limitation of this study

While our study provides a new structural framework for Huntingtin biology, several limitations remain. First, the specific mHTT-to-wtHTT ratio likely influences the degree of functional deficiency in the polyQ-Golgi complex, yet the precise incorporation pattern of mHTT into the polyQ assemblies remains to be determined. Second, while we characterized the fragility of polyQ assemblies under stress in HD cells, it is unclear how this structural instability relates to the subsequent nuclear deposition of polyQ. Future studies utilizing super-resolution and longterm imaging in the living HD cells may be required to visualize the real-time assembly and transition of these complexes into nuclear inclusions.

Materials and methods

Ethics

The ethics of this HD work was approved (No. 28) by the Ethics Committee of the Institutes of Biomedical Sciences at Fudan University. All HD family members who participated in this study signed a written consent form translated into Mongolian and consent to enter this study and authorisation for publication has been obtained. Dr. Li Li collected the human brain samples.

The ethics approval number was obtained from the Huashan Hospital Ethics Committee (KY2018-310.01).

Human fibroblast and blood sample collection

After obtaining consent, a surgeon collected skin samples from the upper arm using a Skin Punch (diameter, 0.3 x 0.3 cm). After collecting samples, a nurse and doctor visited the patients daily for 7 days to prevent inflammation. The tissues were harvested into a tube with culturing medium supplied with antibiotics. After being transported to a lab, tissues were moved to a Biosafety Cabinet, sliced into smaller fragments with surgical knives, and then attached to dishes with forceps and cultured in a small amount of medium. After fully attaching to dishes, the tissues were placed in sufficient medium and cultured continuously for several weeks to obtain sufficient fibroblasts.

Data availability

The sequencing datasets generated and/or analyzed during this study are available in the Sequence Read Archive (SRA) and Gene Expression Omnibus (GEO) with the following accession numbers for anyone: Day 60 and Day 80 MSN in hStrO for bulk RNA-seq (PRJNA760260), Day 110 MSN culture in hStrO for scRNA-seq (GSE184255).

Supplementary Materials and Methods

Primer and sequencing

A nurse collected blood from the upper arm vein, and a Blood DNA Isolation Kit extracted blood DNA. After PCR amplification, the mutant band separates from the wild-type band on a 4% Agarose gel, and the band is then cut and extracted using a DNA Gel Extraction Kit (GenElute™, Sigma-Aldrich). The extract was sequenced by the Sanger method.

The sequencing primers:

A1: 5’-CAGAGCCCCATTCATTGCC-3’

B1: 5’-TGAGGAAGCTGAGGAGGC-3’

Glucose starvation assays for polyQ assemblies and Golgi

Cultured the fibroblasts in a 24-well plate with cover glasses (Φ20mm). After two days, the medium was replaced by low-glucose medium without FBS. The cells in low-glucose medium were fixed at 24 h, 48 h, and 72 h, and stained with the 3B5H10 antibody and phalloidin. At 72 h, the medium was replaced with high-glucose medium lacking FBS and cultured for an additional 48 h, then fixed and stained with 3B5H10 antibody and phalloidin. ImageJ software was used to measure the polyQ assemblies. Imaris was used to render the image. A group of fibroblasts was stained by GM130 antibodies at 48 h after supplying low-glucose medium for Golgi changes.

Onjisaponin and ASO treatments

The sequence of HuASO: 5’-CTCAGtaacattgacACCAC-3’. 5mg HuASO were synthesized by WuXi AppTec. ASOs were solubilized in 0.9% sterile saline solution or PBS. Onjisaponin F was purchased from Jindu Biotech of Shanghai and dissolved in DMSO to a concentration of 100 mM.

Brain organoids (day 100) were treated continuously for 10 days with ASOs at final concentrations of 40 μg/mL. And fibroblasts were treated continuously for 5 days with ASOs at final concentrations of 20, 40 μg/mL. Vehicle (PBS) were used as controls. ASOs were solubilized in sterile PBS and supplemented directly into the culture medium, with media and ASO replenishment every 24 hours.

Immunostaining

Cells, tissues, or organoids were fixed in fresh ice-cold 4% PFA for 15-30 minutes and overnight, respectively. After fixation, immunostaining was performed as previously described[1]. Primary antibodies were used as follows: anti-Tuj-1 antibodies (mouse, Sigma, T8860, 1:5000; rabbit, Covance Research Products, PRB-435P, 1:5000), 3BH10 antibody (Mouse, Sigma, P1874, 1:10000), anti GABA antibodies (rabbit, Sigma, A2052, 1:5000; mouse; Sigma, A0310, 1:500), Clathrin antibody (Rabbit, Abcam, ab21679, 1:1000), GM130 antibody (Rabbit, Abcam, ab52649, 1:1000), IHC-plus™ Polyclonal Rabbit anti-Human HTT / Huntingtin Antibody (C-Terminus, LS-B11011, 1:200). Secondary antibodies used were as follows: Alexa Fluro 488 Donkey anti-mouse IgG (Invitrogen, Molecular Probe, A21202, 1:1000), Alexa Fluro 594 Donkey anti-mouse IgG (Invitrogen, Molecular Probe, A21203,1:1000), Alexa Fluro 594 Donkey anti-rabbit IgG(Chemicon, A21207,1:1000), Alexa Fluro 488 Donkey anti-rabbit IgG (Invitrogen, Molecular Probe, A21206,1:1000), Alexa Fluro 594 Donkey anti-goat IgG (Invitrogen, Molecular Probe, A11058,1:1000) Cy5 AffiniPure Donkey Anti-Goat IgG (H+L) (Jackson, 705-175-147,1:300), Cy5 AffiniPure Donkey Anti-Rabbit IgG (H+L) (Jackson, 711-175-152,1:300), Alexa Fluo 633 Phalloidin (Invitrogen, A22284,1:200), Mito-Tracker™ Green (Invitrogen, M7514), ER-Tracker™ Green (Invitrogen, E34251), DAPI (Sigma, D9542), Phalloidin Alexa-633 or 488 (ThermoFisher, A12379 or A22284, 1:1000), GOLGI ID® Green assay kit (ENZO, ENZ-51028-K100).

Golgi apparatus-selective staining and imaging in live cells

Replated fibroblasts in glass-bottomed 35mm dishes (biosharp, BS-20-GJM). The Golgi apparatus in live cells was labeled with the GOLGI ID Green assay kit (ENZO, ENZ-51028-K100), a Golgi-selective dye. The Assay Solution and the Detection Reagent according to the manufacturer's guidelines. After preparation, these agents were fully mixed. After washing the cells with Assay Solution, a sufficient volume of Detection Reagent was dispensed to cover the monolayer cells, and the cells were incubated for 30 minutes at 37°C. Before imaging, the cells were washed 3 times and incubated in medium at 37°C for another 30 minutes. For imaging, sequential images were captured from multiple ROIs (regions of interest) in dishes. The time intervals were 30 min, 60 min, 120 min, and 240 min.

2D Neural differentiation

The cells were differentiated according to the neural differentiation protocol described [1]. Briefly, dissociated WT-iPS and HD-iPS cells were plated on Matrigel (BD) at a density of 3.5×104 cells/cm2 and maintained in E8 medium (Thermo Fisher Scientific) for 4-5 days until they reached 90% confluence.

After digestion with EDTA, 9000 cells were plated in each well of U-shaped 96-well plates (SUNILON). On the first day, we maintained these cells in E8 and hNM (1:1 mixture). On the second day, the medium was replaced with hNM. From day 0 to day 6, the medium containing 2 μMol/L SB431542 (Tocris) and 0.3 μMol/L LDN193189 (BMP inhibitor, Tocris) was used for culture. These cells were plated in a well on day 7, and 200 ng/ml SHH or 0.65 μM Purmorphamine was supplied on day 10 for the differentiation of GABAergic neurons. The cells were maintained in the same medium for 2 weeks. The medium without SHH or Purmorphamine is used for differentiating glutamate neurons. At 15 days of differentiation, the rosettes were collected and cultured in a suspension condition for 25 days. On day 25, these cells were plated on a cover glass double-coated by polyonithin and laminin after digesting with accutase and then supplemented by a neural induction medium (composed of Neurobasal, N2 100×, B27 50×) (Invitrogen), supplemented with 10 ng/ml BDNF (Peprotech), 10 ng/ml GDNF (Peprotech) and 10 ng/ml IGF (Peprotech).

Human brain organoid construction

Brain organoids were constructed according to our protocol 2. Briefly, ES/iPS colonies were dissociated into single cells using Accutase (Gibco, A1110501). 9,000 dissociated cells were plated into each well of a V-bottom ultra-low-attachment 96-well plate (Sumitomo Bakelite, MS-9096VZ). Induction media contained Human Neural differentiation Medium and E8 media (1:1), supplemented with the two SMAD inhibitors 0.3μM LDN-193189 (STEMGENT, 040074), 2μM SB431542 (Ametek Scientific, DM-0970), and 10 μm Y-27632 (APE.BIO, A3008). On the sixth day in suspension, hCOs were transferred to neural differentiation media containing a 1:1 mixture of DMEM-F12 media and Neurobasal media supplemented with 1% (v/v) MEM-NEAA (Gibco, 11140-050), 1% (v/v) GlutaMAX(Gibco, 35050-061), 1% (v/v) N2 supplement (Gibco, 17502-048), 2% (v/v) B27 supplement (Gibco), 1% (v/v) Penicillin/Streptomycin (Gibco, 2051357). Growth factors 10ng/ml EGF (R&D Systems, 236-EG) and 20 ng/ml bFGF (R&D Systems, 233FB/CF) were used from day6 to day23. Growth factors, the 20 ng/ml BDNF (Peprotech, AF450002) and 10 ng/ml GDNF (Peprotech, AF450010) were used from day 24 to day 45.

Interfacing the brain organoid with HD-MEA

To facilitate robust hCO-electrode coupling, high-density microelectrode array (HD-MEA) chips (Maxlab Biosystems, Switzerland) were first functionalized. The sensing area was treated with a 0.07% (v/v) poly(ethylenimine) (PEI; Sigma-Aldrich) solution followed by a coating of laminin. For the interfacing of hCOs, we adapted the manufacturer's protocols for brain slices. Individual hCOs were meticulously transferred to the center of the coated electrode arrays. To ensure mechanical stability and intimate contact between the basal surface of the organoid and the electrodes, a small droplet of Matrigel (Corning) was applied to secure the tissue. The chips were then lidded and incubated at 37 °C with 5% CO2 for 30 minutes to allow for matrix gelation. Subsequently, the culture was replenished with BrainPhys neuronal medium (StemCell Technologies) supplemented with the following reagents: 2% (v/v) NeuroCult SM1 Neuronal Supplement (StemCell Technologies), 1% (v/v) N2 Supplement-A (Gibco), 1x GlutaMAX (Gibco), 20 ng/ml recombinant human BDNF, 20 ng/ml recombinant human GDNF (PeproTech), 20 ng/ml NT-3 (PeproTech), 1 mM dibutyryl-cAMP (Sigma-Aldrich), and 1x Antibiotic-Antimycotic (Gibco). The recording medium was changed every 2–3 days.

Electrophysiological recordings

To probe network activity in hCOs, longitudinal HD-MEA recordings were used. The spontaneous activity was recorded sequentially in blocks across the entire array (30 seconds per recording configuration, each comprising 1020 recording electrodes). Signals were sampled at 20 kHz for all recordings and saved in an HDF5 file format. Spike detection was performed using a threshold set to 5× the root-mean-square (RMS) of the noise in the band-pass-filtered signal. After the activity scan, the readout electrodes were selected depending on the requirements of each analysis (single-cell or network-related features). All HD-MEA recordings of hCOs started at least 7 days after plating. The reported electrophysiological results are based on data obtained from n=3 hCOs (CTR group), n=3 hCOs (HD group), and n=3 hCOs (HD group with ASO treatment).

Preparation and data analysis of a single-cell RNA-sequencing library

110 days differentiated hStrOs from a HD patient (CAG 59), a healthy sibling, and H9 in suspension culture are prepared for analysis. A sterile dish with 10 ml 1x Dulbecco's Phosphate-Buffered Saline (DPBS; Thermo Fisher, 14190144) on ice is used to transport samples after removing the residual solution. Neurosphere Dissociation Kit (Miltenyi, 130-095-943) used to create single-cell suspensions. Dissociated cells were rinsed 1x DPBS containing 2% FBS. 0.4% Trypan blue staining (Thermo Fisher, 14190144) is used to assess viability on the Countess® II Automated Cell Counter (Thermo Fisher).

10x library preparation and sequencing

Beads with unique molecular identifier (UMI) and cell barcodes were loaded close to saturation, so that each cell was paired with a bead in a Gel Beads-in-emulsion (GEM). After exposure to cell lysis buffer, polyadenylated RNA molecules hybridized to the beads. Beads were retrieved into a single tube for reverse transcription. For cDNA synthesis, each cDNA molecule was tagged at the 5' end (i.e., the 3' end of a messenger RNA transcript) with a UMI and a cell label indicating its cell of origin. Briefly, 10× beads that were then subject to second-strand cDNA synthesis, adaptor ligation, and universal amplification. Sequencing libraries were prepared from randomly interrupted whole-transcriptome amplification products to enrich for the 3' ends of transcripts linked to the cell barcode and UMI. All remaining procedures, including library construction, were performed according to the manufacturer's standard protocol (Chromium Single Cell 3′v3). A High Sensitivity DNA Chip (Agilent) on a Bioanalyzer 2100 and the Qubit High Sensitivity DNA Assay (Thermo Fisher Scientific) quantified NovaSeq6000 (Illumina) sequencing libraries (2x150 chemistry).

Single cell RNA-seq data processing and analysis

Cell Ranger 4.0 pipeline with default and recommended parameters processed the reads. Gene-Barcode matrices were generated for each sample by counting UMIs and filtering out non-cell-associated barcodes, and a gene-barcode matrix containing the barcoded cells and gene expression counts was generated. After obtaining the single-cell expression matrix, we used the Seurat (v4.0.5)[2] R toolkit to perform normalization, clustering, dimensionality reduction, and visualization. Cells that had the number of detected genes less than 200 and the percentage of mitochondrial genes lower than 10% were removed. Gene counts were then log-transformed and scaled, and 3000 shared highly variable genes were identified using the FindVariableFeature function. We applied the Runharmony function with the Seurat-based principal component analysis (PCA) reduction method in the Harmony (v0.1.0)[3] package to correct batch effects and generate low-dimensional matrices. A nearest-neighbor graph was calculated using FindNeighbors and clustered using FindClusters, followed by visualization of the cell clusters using uniform manifold approximation and projection (UMAP). We used the well-known marker genes to assign these clusters to corresponding cell types. Differentially expressed genes(|log2FC|>0.25 and adjusted p value<0.01) among GABAergic neurons (CAG 59 vs CAG 19, CAG 59 vs H9) were identified by the Seurat function FindMarkers.

Functional enrichment

Enrichment GO categories for significantly differentially expressed genes were identified by Metascape (*https://metascape.org/gp/*)[4], which utilizes hypergeometric test and Benjamini-Hochberg p-value correction algorithm to identify acceptable ontology terms. Adjusted p value of GO biological processes <0.01 was considered to be significant enrichment terms. The gene set enrichment score of Golgi vesicle transport (GO:0048193) was calculated by AUCell(v.1.14.0)[5]. The AUCell_buildRankings and AUCell_calcAUC algorithms were used for ranking model building and calculating "Area Under the Curve" (AUC) scores.

LC-MS analysis

The patients' iPSCs were differentiated for 50 or 100 days, and the samples were then sent to the core facility of the State Key Laboratory of Genetic Engineering for analysis. The FASP digestion was adapted for the following procedures in Microcon PL-10 filters. After a three-time buffer displacement with 8 M Urea and 50 mM ABC, pH 8.5, proteins were reduced by 10 mM DTT at 37 °C for 30 min, followed by alkylation with 30 mM iodoacetamide at 25 °C for 45 min in a light-proof condition. Digestion was performed with trypsin (enzyme/protein ratio 1:50) at 37 °C for 12 h, after which the sample was rinsed with 20% ACN and buffer displaced three times with digestion buffer (10 mM ABC). After digestion, the solution was filtered, the filter rinsed twice with 15% ACN, and the filtrates were pooled and vacuum-dried. LC-MS analysis was performed using a nanoflow EASYnLC 1200 system (Thermo Fisher Scientific, Odense, Denmark) coupled to an Orbitrap Exploris 480 mass spectrometer (Thermo Fisher Scientific, Bremen, Germany). A one-column

system was adopted for all analyses. A home-made C18 analytical column (75 μm i.d. × 25 cm, ReproSil-Pur 120 C18-AQ, 1.9 μm (Dr. Maisch GmbH, Germany) was used to analyze samples. The mobile phases are composed of Solution A (0.1% formic acid) and Solution B (0.1% formic acid in 80%ACN).

The derivatized peptides were eluted using the following gradients: 5–8% B in 2 min, 8–44% B in 98 min, 44–60% B in 3 min, 60–100% B in 2 min, 100% B for 10 min, at a flow rate of 200 nL min. High-field asymmetric-waveform ion mobility spectrometry (FAIMS) was enabled during data acquisition, with compensation voltages set to −45 and −65 V. MS1 data were collected in the Orbitrap (60,000 resolution). Charge states 2-7 were required for MS2 analysis, and a 45 s dynamic exclusion window was used. Cycle time was set at 1.5 s. MS2 scans were performed in the Orbitrap with HCD fragmentation (isolation window 1.6; 15,000 resolution; NCE 30%).

Extended Data

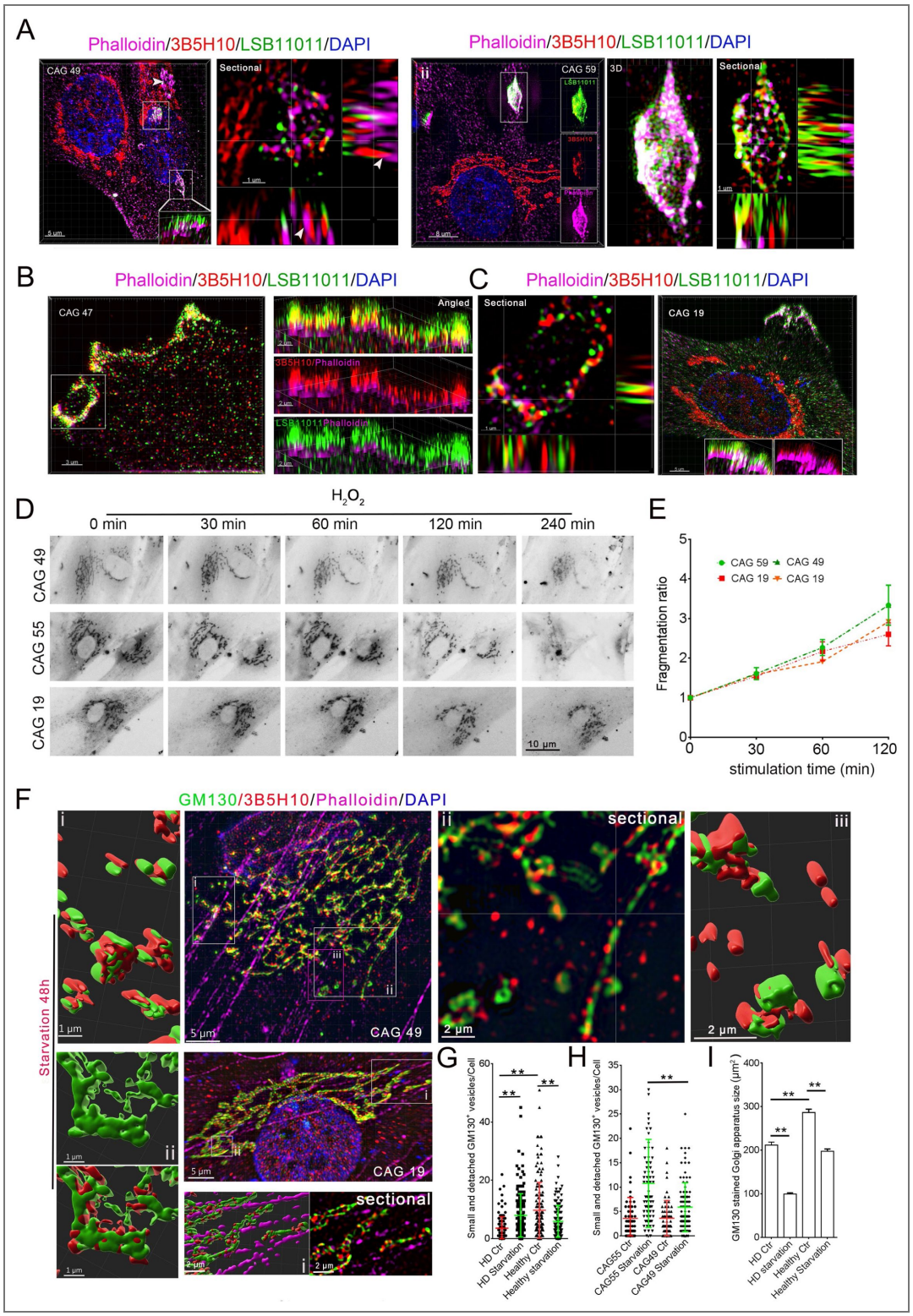

Figure S1. Characterization of polyQ assemblies and Golgi activities A. LSB11011 (C-terminal of HTT) and 3B5H10 (N-terminal) antibody and phalloidin immunostaining revealed that actin filaments are enriched on the edge of large polyQ assemblies (i) or some small polyQ assembly near the cellular membrane (ii) (the boxed region indicated the sectional view in the right panel; white arrows, the polyQ assemblies interact with actin; the inner panels in ii are the spliced channels; white arrows, the interacting patterns of polyQ with F-actin). **B, C.**

LSB11011 (C-terminal of HTT) and 3B5H10 (N-terminal) antibodies, and phalloidin immunostaining revealed a linear assembly of polyQ on the ruffling membrane. The right panel shows a 3D image (B) revealing the alignment pattern of polyQ on membrane curvature and ruffling membrane. The image of sectional views (C) revealed the interaction pattern of polyQ with actin filaments. **D.** Image sequences of the Golgi in the fibroblasts of the HD family under oxidative stress at the indicated time points. **E.** The fragmentation ratio of the Golgi under H2O2 stimulation at different time points. Fragmentation ratio = number of Golgi of one cell at each time point/ number of Golgi at 0 min. Two-way ANOVA. *<0.05; **<0.01.D **F.** The images of 3B5H10 and GM130 antibody immunostaining in the fibroblasts after 48 h glucose starvation, taken by SIM microscopy. The 3D-rendered tomography showed the spatial relationship between polyQ assemblies/puncta and the Golgi. The boxed regions are the magnified part or rendered region. **G, H.** The changes of Golgi fragments after 48 h glucose starvation in the fibroblasts of healthy siblings (two siblings, CAG 19) and HD patients (CAG 55 and CAG 49). HD/healthy ctr, the fibroblasts cultured in high glucose medium; HD/healthy starvation, the fibroblasts cultured in low glucose medium for 48h. Two-way ANOVA; **0.01. Cell count in each group: n>120. **I.** The changes of GM130-stained Golgi sizes after 48 h glucose starvation in the fibroblasts of healthy siblings (two, CAG 19) and HD patients (CAG 55 and CAG 49). HD/healthy ctrl, the fibroblasts cultured in high glucose medium; HD/healthy starvation, the fibroblasts cultured in low glucose medium for 48h. One-way ANOVA; **0.01. The number of images in the cell line: n>20. Cell count in each group: n>400.

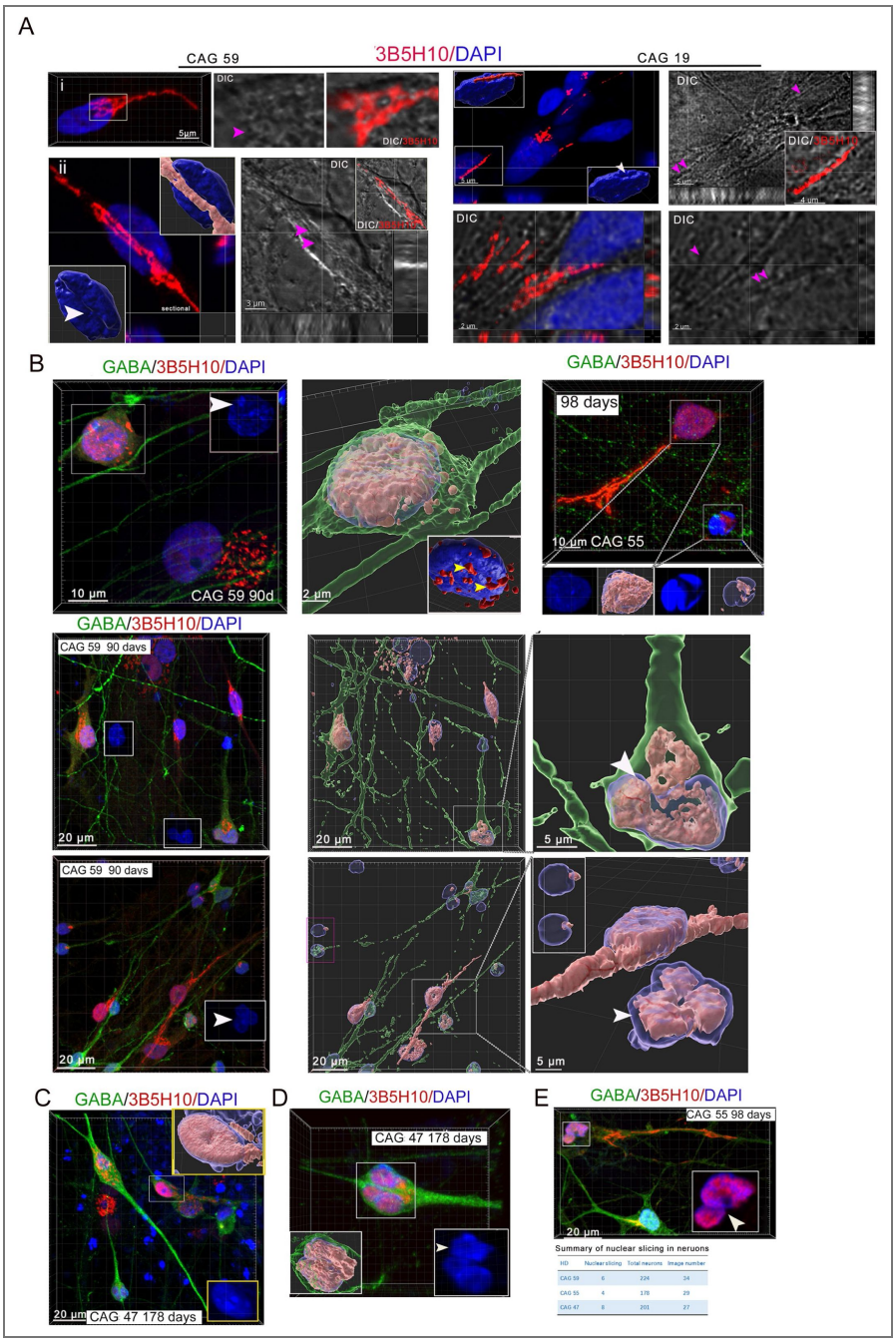

Figure S2. Characterization of endogenous polyQ aggregate structure

A. 3B5H10 antibody and phalloidin staining showed polyQ distribution patterns in the fibroblasts of healthy (CAG 19) and patient (CAG 59). 3D-reconstructed tomography by IMARIS revealed the spatial relationships between polyQ assemblies and the nuclear surface and F-actin filaments (white arrows, polyQ puncta within the nucleus; yellow arrows, nuclear interactions). The yellow arrows in the DAPI-rendered image indicated the nuclear surface. **B.** The size of polyQ assemblies in the fibroblasts of healthy siblings (n=4; cells, n=306) and HD patients (n=4; CAGs: 59, 55, 49, and 47; cells, n=783). Fiji ImageJ measured the size. **C.** Average size of polyQ assembly in HD patients and healthy siblings. Student t-test; ns, p >0.05. **D.** Mito-tracker, phalloidin, and 3B5H10 antibody immunostaining in the fibroblasts of HD patients (CAGs, 49) and healthy siblings. 3D rendering tomography in the right two panels revealed the spatial relationships of polyQ assemblies with mitochondria and actin filaments. **E.** 3B5H10 (three rights) or 3B5H10 (N-terminal) and LSB11011 (C-terminal) (left) stained polyQ puncta/patches in the mitotic cells. **F.** The representative image of 3B5H10 antibodies immunostaining in HD patient (CAG 44) and healthy sibling fibroblasts by two different protocols (immediate staining is stained 15-30 minutes after 4% PFA fixation; delayed staining is stained 48 h after 4% PFA fixation). Left panels show freshly fixed and immediately stained groups; right panels show freshly fixed and later stained groups. Images were taken by SIM microscopy with Z-stacks.

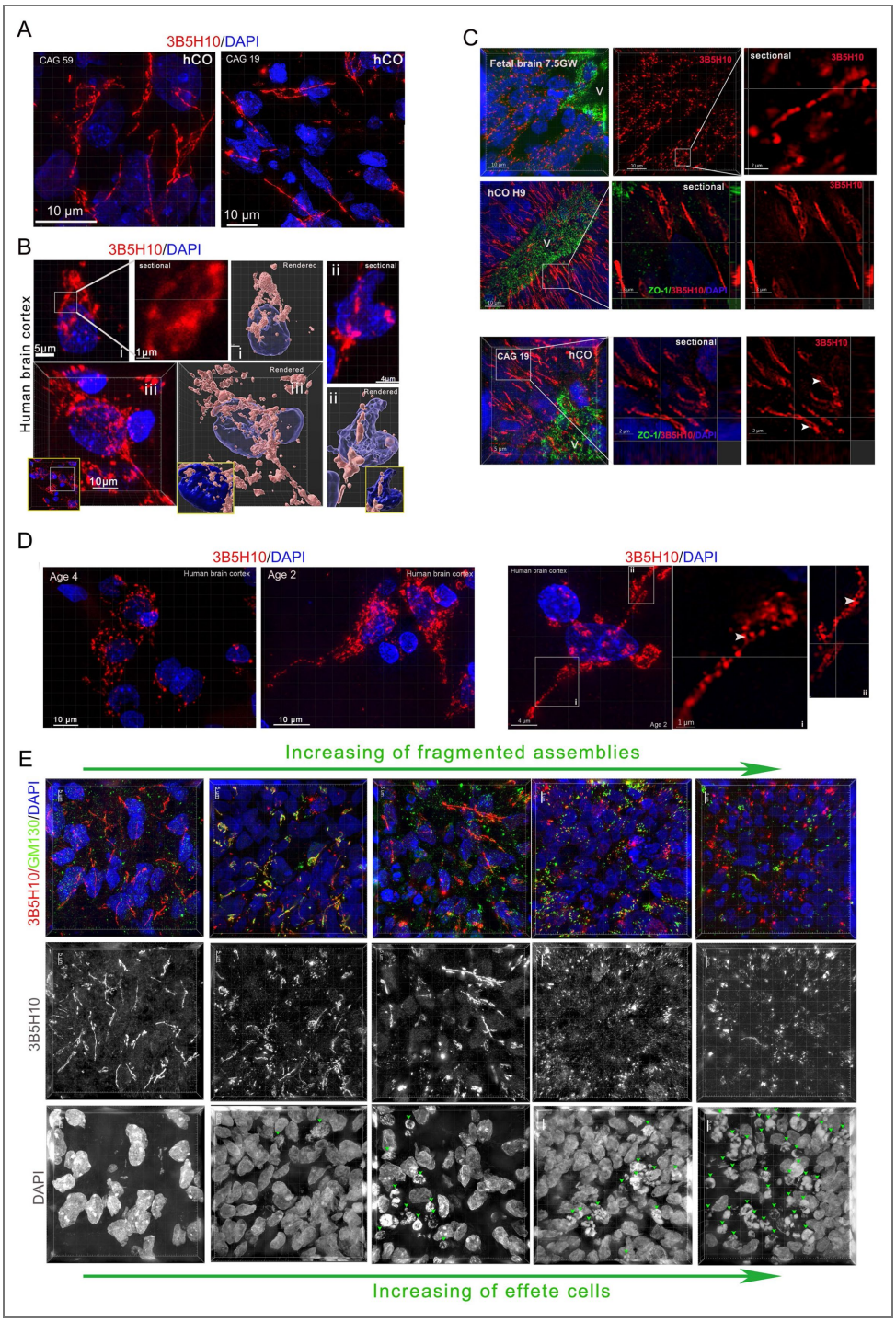

Figure S3. PolyQ assemblies in human fetal and child brains and human brain organoids with necrotic cells

A. Typical appearance of intact and continuous polyQ assemblies in the neurons of hStrO. **B.** PolyQ assemblies stained by 3B5H10 antibody in fresh surgical brain tissues collected from a 4-year-old glioblastoma patient. Three representative appearances of polyQ assemblies in human brain cells. The middle panel (image-i) is a sectional view that shows a ring-like structure; the left corner insert in image-ii is a larger view; the rendered tomography shows the nuclear surface. **C.** 3B5H10 and ZO-1 antibodies immunostained intact polyQ assemblies in the pseudostratified neuroepithelium of the neural tube in the human fetal brain at 7.5 gestation weeks, and hCOs from HD patients, H9, and healthy siblings showed that the polyQ assemblies in the neuroepithelial cells are intact and long and formed by a small ring-like unit, and paralleled the apical-basal axis of cells. **D.** Fragmented/discontinuous polyQ assemblies in freshly surged human brain samples from cortex (tissues from 4-year-old and 2-year-old glioblastoma patients). **E.** The fragmentation of polyQ assemblies depends on the necrotic cells in the surrounding regions (green arrows, necrotic cells).

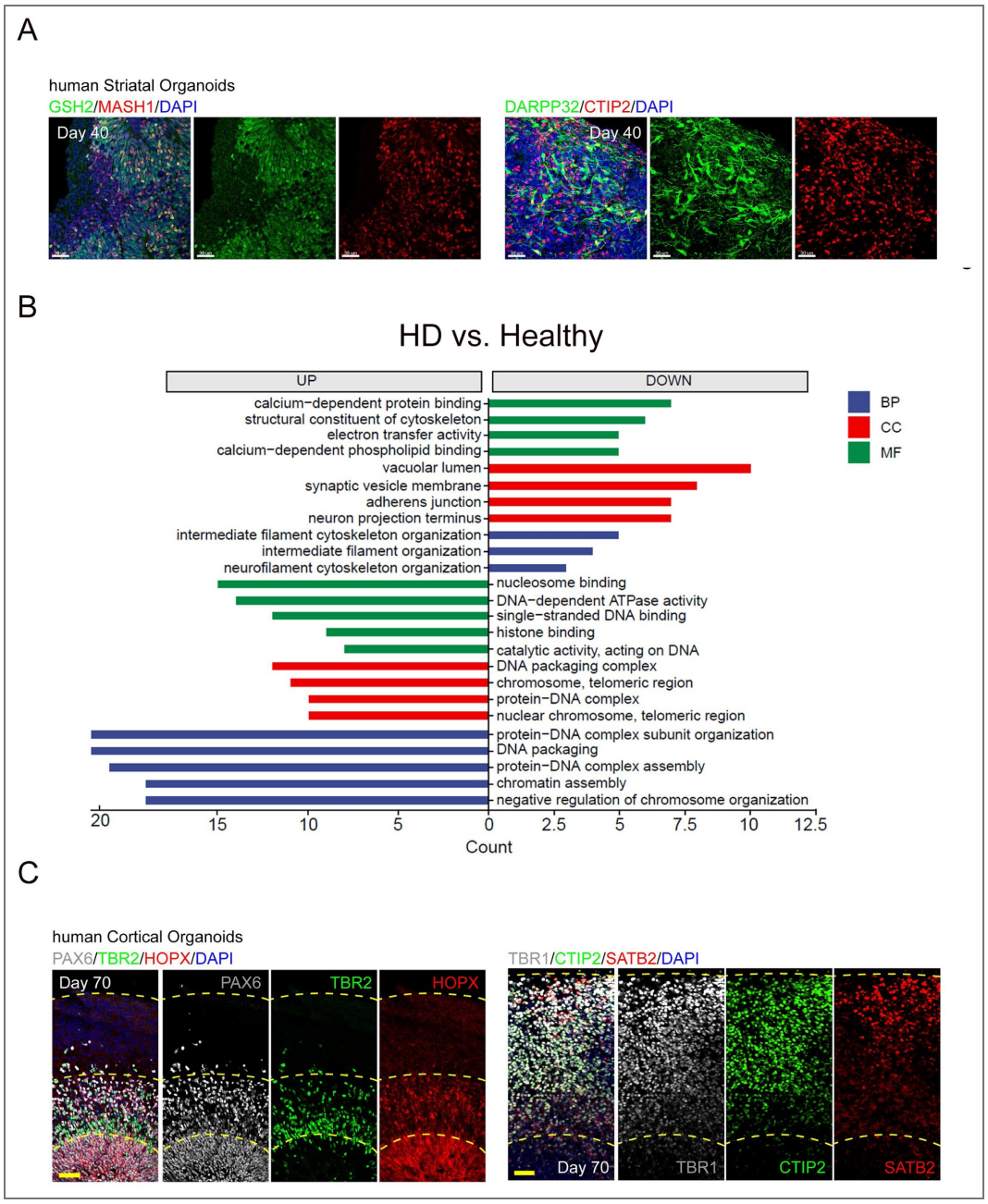

Figure S4. The impaired nuclear activities in HD striatal organoids

A. The validation of hCO and hStrOs by immunostaining with GSH2/MASH1 or DARPP321/CTIP2 antibodies. B. GO analysis of differentially expressed proteins in HD striatal neurons derived from iPSCs and healthy GABAergic neurons derived from iPSCs at 60 100 days (CAG 55 vs. H9 and CAG 19). C. The validation of hCO by immunostaining with PAX6/TBR2 /HOPX or TBR1/CTIP2/SATB2 antibodies.

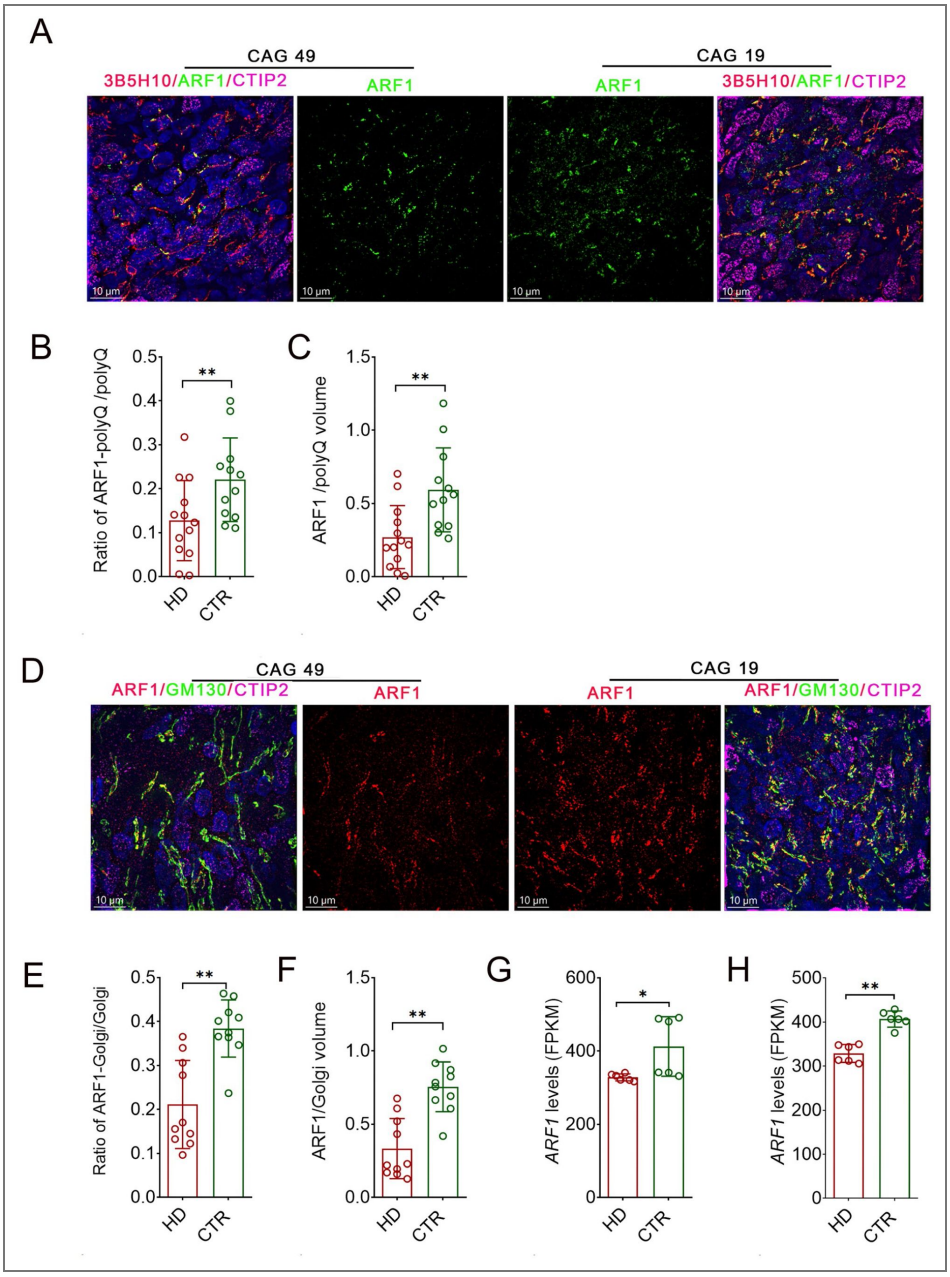

Figure S5. ARF1 levels were reduced in HD neurons

A. The immunostaining results of ARF1, CTIP2, and 3B5H10 antibodies in the neurons of hStrOs (CAG 49 and CAG 19). The middle panels showed ARF1 signals. **B, C.** The overlapped volume of ARF1 with polyQ in the HD and healthy neurons of hStrOs (G). The ratio of ARF1 volume/polyQ volume in CTIP2 + regions. The surface function of IMARIS was used to calibrate volume. Object-object statistics in IMARIS measure the overlapped volume. t-test, *<0.05; **<0.01. D. The immunostaining results of ARF1, CTIP2, and GM130 antibodies in the neurons of hStrOs (CAG 49 and CAG 19). The middle panels showed ARF1 signals. **E, F.** The overlapped volume of ARF1 with the Golgi in the HD and healthy neurons of hStrOs. The ratio of ARF1 volume/Golgi volume in CTIP2 + regions. The surface function of IMARIS was used to calibrate volume. Object-object statistics in IMARIS measure the overlapped volume. t-test, **, p<0.01. **G.** Bulk RNAseq data of HD hStrOs (CAG 55 and 59) and healthy hStrOs (CAG 19 and H9) at 60 days revealed *ARF1* transcription levels. *Student t-test; *<0.05; **<0.01*. **H.** The bulk RNAseq data of HD hStrOs (CAG 55 and 59) and healthy hStrOs (CAG 19 and H9) at 80 days revealed *ARF1.* Student t-test; **, *p<0.01.* CTR, healthy.

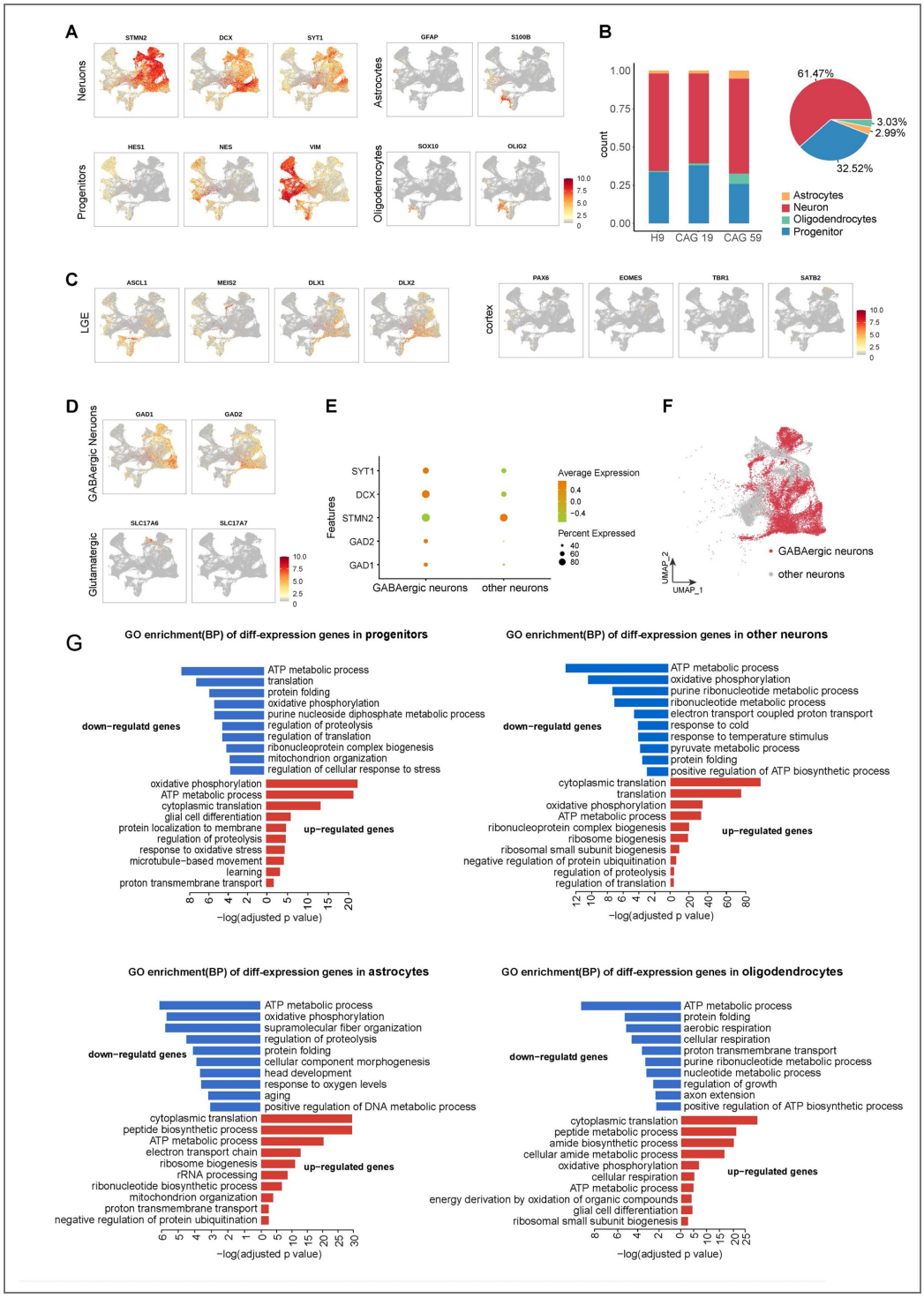

Figure S6. Characterizing and sorting the cellular types from scRNA-seq data of hStrOs and GO analyses of different cellular clusters in scRNA-seq data of hStrOs

A. Expression of known markers of progenitor, neuron, astrocyte and oligodendrocyte. B. Stacked bar plots and a pie chart representing the proportion of cell types. C, D. Expression of known markers of LGE progenitors and cortical progenitors(C), GABAergic neurons and glutamatergic neurons (D). E. Dot plot displaying expression of GABAergic neurons marker genes. F. UMAP plot of neurons colored by GABAergic neurons (red) and other neurons (grey). G. GO enrichment analysis of down-regulated (top) and up-regulated (bottom) genes in CAG59 VS CAG19/H9 progenitor, other neuron, astrocyte, and oligodendrocyte.

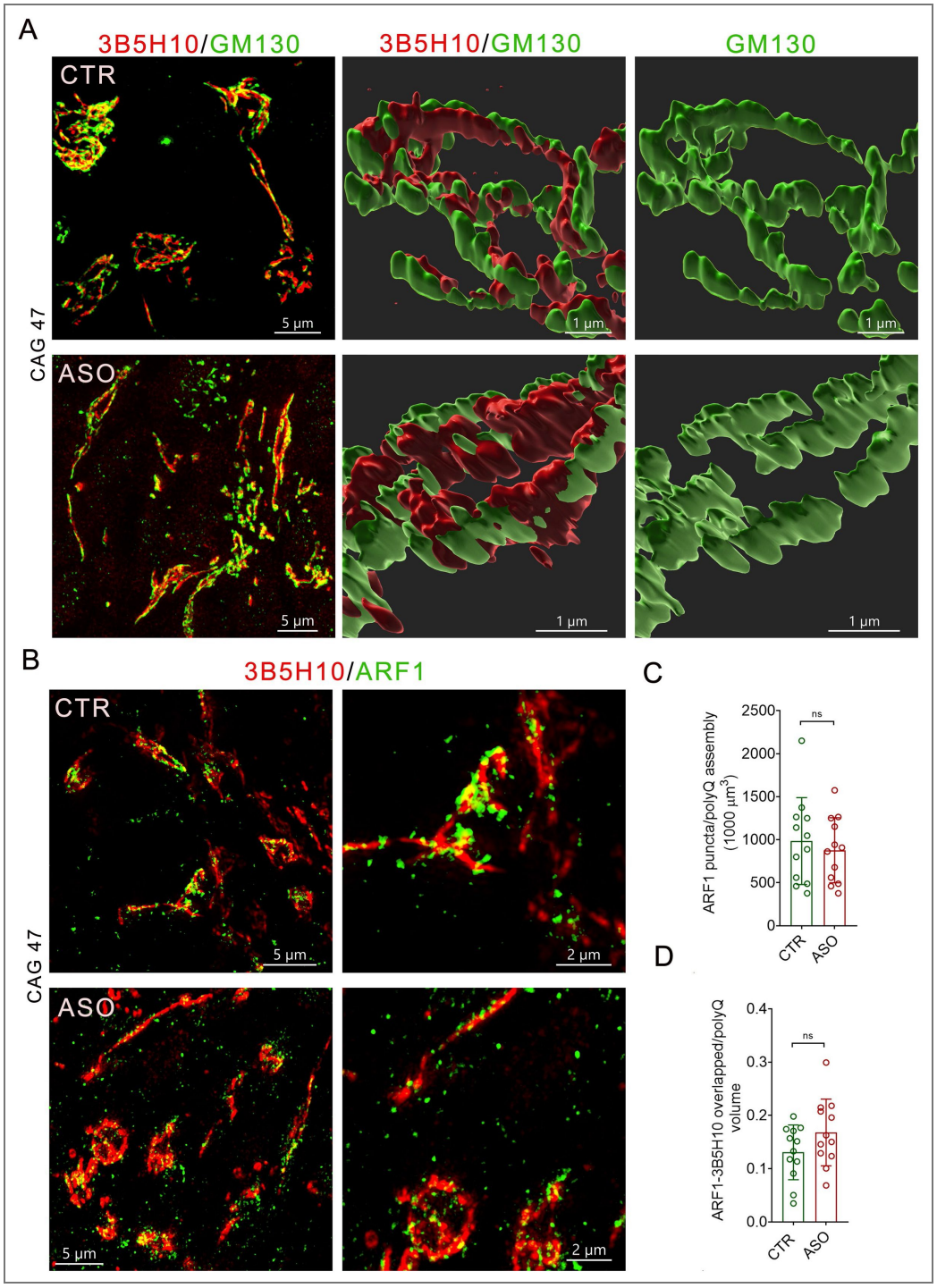

Figure S7. ASO treatments did not alter Golgi morgphology and ARF1 scaffolding in polyQ assembly

A. The representative super-resolution images of polyQ assemblies stained by 3B5H10 antibody and Golgi stained by GM130 antibody in ASO-treated and control h hCOs. The middle and right panels show the spatial relationships between polyQ assemblies and the Golgi, and the tomography of the Golgi, respectively. The renderings are done by IMARIS surface. **B.** The representative super-resolution images of polyQ assemblies stained by 3B5H10 antibody and ARF1 puncta in ASO-treated and control (CTR) hCOs. The images are displayed as MIP. The rights are the magnified region in the rectangle on the left. **C.** The density of ARF1+ puncta in polyQ assemblies ASO-treated and control (CTR) hCOs (HD, n=2 [CAG 47 and CAG 59]; hCOs, n=6; t-test, ns>0.05). Puncta are counted with the IMARIS surface. **D.** The overlapped volume of ARF1 puncta with polyQ assemblies in ASO-treated and control (CTR) hCOs. (HD, n=2 [CAG 47 and CAG 59]; hCOs, n=6; t-test, ns>0.05). polyQ assembly and puncta volume are measured by the IMARIS surface.

No	Gender	Age	F	Onset age	CAG (mutant)	CAG (wild)	Syndrome (on sampling age)	Death	Sampling year
1	F	46	F3	42	47	19	moderate		2010
2	M	44	F3	37	49	19	moderate	54	2010
3	M	21	F4			19			2010
4	F	28	F4			19			2010
5	F	26	F4			19			2010
6	M	23	F4	26	57	19	mild		2010
7	M	27	F4	23	59	19	mild	36	2010
8	F	19	F4			19			2010
9	M	28	F4	30	48	19	mild		2010
10	F	26	F4	32	47	19	no syndrome		2010
11	M	5	F5		45	18	no syndrome		2010
12	F	39	F4	30	55	19	critical	42	2010
13	F	42	F4			19			2010
14	F	23	F4			19			2010
15	M	44	F4	41	NA		critical		2010
16	M	17	F5		NA				2010
17	M	33	F4			19			2017
18	F	30	F3		45	19	no syndrome		2017
19	F	52	F4		45	19	moderate		2017
20	F	25	F3			19			2017
21	M	21	F3			19			2017
22	M	52	F2		NA		died without syndrome		2019
23	M	30	F4		44	19	no syndrome		2019
24	F	54	F3		42	19	moderate		2019
25	F	56	F3		NA		critical		2020
26	M	52	F3		NA		healthy		2020
27	F	28	F4		NA		healthy		2020
28	M	32	F4		NA		healthy		2020

F, female; M, male; NA, non-assessed; F1-4 genereation

Table S1. **The baseline characteritics of HD family members.**

Additional information

Author contributions

HS and LM set up this study. HS and LM performed most of the experiments; HS analyzed the data and prepared the manuscripts; XC, WY, YL, BH, and JX performed image analysis and immunostaining. XC, LY, and LM constructed organoids.

Financial supports

This work was supported by the National Natural Science Foundation of China (grant no. 32370852 and U24A2014 to LM) and the National Key Research and Development Program of China (grant no. 2021YFA1101302 to LM)

Funding

Funder	Grant reference number	Author
MOST | National Natural Science Foundation of China (NSFC)	2370852	Lixiang Ma
MOST | National Natural Science Foundation of China (NSFC)	U24A2014	Lixiang Ma
MOST | National Key Research and Development Program of China Stem Cell and Translational Research (Stem Cell and Translational Research)	2021YFA1101302	Lixiang Ma

Author ORCID iDs

Li Li: https://orcid.org/0000-0002-2374-5203
Jianzhong Su: https://orcid.org/0000-0003-1054-6042
Hexige Saiyin: https://orcid.org/0000-0003-2993-6817

References

Arrasate M., Mitra S., Schweitzer E.S., Segal M.R., Finkbeiner S (2004) Inclusion body formation reduces levels of mutant huntingtin and the risk of neuronal death. *Nature* **431**:805-810 https://doi.org/10.1038/nature02998 | PubMed

Barnat M., Capizzi M., Aparicio E., Boluda S., Wennagel D., Kacher R., Kassem R., Lenoir S., Agasse F., Braz B.Y., *et al.* (2020) Huntington's disease alters human neurodevelopment. *Science* **369**:787-793 https://doi.org/10.1126/science.aax3338 | PubMed

Bauerlein F.J.B., Saha I., Mishra A., Kalemanov M., Martinez-Sanchez A., Klein R., Dudanova I., Hipp M.S., Hartl F.U., Baumeister W., *et al.* (2017) In Situ Architecture and Cellular Interactions of PolyQ Inclusions. *Cell* **171**:179-187. https://doi.org/10.1016/j.cell.2017.08.009 | PubMed

Caviston J.P., Ross J.L., Antony S.M., Tokito M., Holzbaur E.L (2007) Huntingtin facilitates dynein/dynactin-mediated vesicle transport. *Proc Natl Acad Sci U S A* **104**:10045-10050 https://doi.org/10.1073/pnas.0610628104 | PubMed

Caviston J.P., Zajac A.L., Tokito M., Holzbaur E.L (2011) Huntingtin coordinates the dynein-mediated dynamic positioning of endosomes and lysosomes. *Mol Biol Cell* **22**:478-492 https://doi.org/10.1091/mbc.e10-03-0233 | PubMed

Chen X., Saiyin H., Liu Y., Wang Y., Li X., Ji R., Ma L. (2022) Human striatal organoids derived from pluripotent stem cells recapitulate striatal development and compartments. *Plos Biol* **20**:e3001868 https://doi.org/10.1371/journal.pbio.3001868 | PubMed

Costa V., Giacomello M., Hudec R., Lopreiato R., Ermak G., Lim D., Malorni W., Davies K.J., Carafoli E., Scorrano L (2010) Mitochondrial fission and cristae disruption increase the response of cell models of Huntington's disease to apoptotic stimuli. *EMBO Mol Med* **2**:490-503 https://doi.org/10.1002/emmm.201000102 | PubMed

D'Souza-Schorey C., Chavrier P. (2006) ARF proteins: roles in membrane traffic and beyond. *Nat Rev Mol Cell Biol* **7**:347-358 https://doi.org/10.1038/nrm1910 | PubMed

del Toro D., Alberch J., Lazaro-Dieguez F., Martin-Ibanez R., Xifro X., Egea G., Canals J.M (2009) Mutant huntingtin impairs post-Golgi trafficking to lysosomes by delocalizing optineurin/Rab8 complex from the Golgi apparatus. *Mol Biol Cell* **20**:1478-1492 https://doi.org/10.1091/mbc.e08-07-0726 | PubMed

del Toro D., Canals J.M., Gines S., Kojima M., Egea G., Alberch J (2006) Mutant huntingtin impairs the post-Golgi trafficking of brain-derived neurotrophic factor but not its Val66Met polymorphism. *J Neurosci* **26**:12748-12757 https://doi.org/10.1523/jneurosci.3873-06.2006 | PubMed

DiFiglia M., Sapp E., Chase K., Schwarz C., Meloni A., Young C., Martin E., Vonsattel J.P., Carraway R., Reeves S.A., *et al.* (1995) Huntingtin is a cytoplasmic protein associated with vesicles in human and rat brain neurons. *Neuron* **14**:1075-1081 https://doi.org/10.1016/0896-6273(95)90346-1 | PubMed

DiFiglia M., Sapp E., Chase K.O., Davies S.W., Bates G.P., Vonsattel J.P., Aronin N (1997) Aggregation of huntingtin in neuronal intranuclear inclusions and dystrophic neurites in brain. *Science* **277**:1990-1993 https://doi.org/10.1126/science.277.5334.1990 | PubMed

Dougan L., Li J., Badilla C.L., Berne B.J., Fernandez J.M (2009) Single homopolypeptide chains collapse into mechanically rigid conformations. *Proc Natl Acad Sci U S A* **106**:2605-12610 https://doi.org/10.1073/pnas.0900678106 | PubMed

Dragatsis I., Efstratiadis A., Zeitlin S (1998) Mouse mutant embryos lacking huntingtin are rescued from lethality by wild-type extraembryonic tissues. *Development* **125**:1529-1539 https://doi.org/10.1242/dev.125.8.1529 | PubMed

Duyao M.P., Auerbach A.B., Ryan A., Persichetti F., Barnes G.T., McNeil S.M., Ge P., Vonsattel J.P., Gusella J.F., Joyner A.L., *et al.* (1995) Inactivation of the mouse Huntington's disease gene homolog Hdh. *Science* **269**:407-410 https://doi.org/10.1126/science.7618107 | PubMed

El Ghouzzi V., Boncompain G. (2022) Golgipathies reveal the critical role of the sorting machinery in brain and skeletal development. *Nat Commun* **13**:7397 https://doi.org/10.1038/s41467-022-35101-y | PubMed

Fasano G., Muto V., Radio F.C., Venditti M., Mosaddeghzadeh N., Coppola S., Paradisi G., Zara E., Bazgir F., Ziegler A., *et al.* (2022) Dominant ARF3 variants disrupt Golgi integrity and cause a neurodevelopmental disorder recapitulated in zebrafish. *Nat Commun* **13**:6841 https://doi.org/10.1038/s41467-022-34354-x | PubMed

Ferrante R.J., Gutekunst C.A., Persichetti F., McNeil S.M., Kowall N.W., Gusella J.F., MacDonald M.E., Beal M.F., Hersch S.M (1997) Heterogeneous topographic and cellular distribution of huntingtin expression in the normal human neostriatum. *J Neurosci* **17**:3052-3063 https://doi.org/10.1523/jneurosci.17-09-03052.1997 | PubMed

Grima J.C., Daigle J.G., Arbez N., Cunningham K.C., Zhang K., Ochaba J., Geater C., Morozko E., Stocksdale J., Glatzer J.C., *et al.* (2017) Mutant Huntingtin Disrupts the Nuclear Pore Complex. *Neuron* **94**:93-107. https://doi.org/10.1016/j.neuron.2017.03.023 | PubMed

Guo Q., Bin H., Cheng J., Seefelder M., Engler T., Pfeifer G., Oeckl P., Otto M., Moser F., Maurer M., *et al.* (2018) The cryo-electron microscopy structure of huntingtin. *Nature* **555**:117-120 https://doi.org/10.1038/nature25502 | PubMed

Gutekunst C.A., Li S.H., Yi H., Mulroy J.S., Kuemmerle S., Jones R., Rye D., Ferrante R.J., Hersch S.M., Li X.J (1999) Nuclear and neuropil aggregates in Huntington's disease: relationship to neuropathology. *J Neurosci* **19**:2522-2534 https://doi.org/10.1523/jneurosci.19-07-02522.1999 | PubMed

Harding R.J., Deme J.C., Hevler J.F., Tamara S., Lemak A., Cantle J.P., Szewczyk M.M., Begeja N., Goss S., Zuo X., *et al.* (2021) Huntingtin structure is orchestrated by HAP40 and shows a polyglutamine expansion-specific interaction with exon 1. *Commun Biol* **4**:1374 https://doi.org/10.1038/s42003-021-02895-4 | PubMed

Hatters D.M., Hannan A.J. (2013) *Tandem repeats in genes, proteins, and disease: methods and protocols* New York: Humana Press.

Isas J.M., Langen A., Isas M.C., Pandey N.K., Siemer A.B (2017) Formation and Structure of Wild Type Huntingtin Exon-1 Fibrils. *Biochemistry-Us* **56**:3579-3586 https://doi.org/10.1021/acs.biochem.7b00138 | PubMed

Jimenez-Sanchez M., Licitra F., Underwood B.R., Rubinsztein D.C (2017) Huntington's Disease: Mechanisms of Pathogenesis and Therapeutic Strategies. *Cold Spring Harb Perspect Med* **7** https://doi.org/10.1101/cshperspect.a024240 | PubMed

Kernich C.A. (2002) Huntington's disease. *Neurologist* **8**:207-208 https://doi.org/10.1097/00127893-200205000-00007 | PubMed

Kim J., Moody J.P., Edgerly C.K., Bordiuk O.L., Cormier K., Smith K., Beal M.F., Ferrante R.J (2010) Mitochondrial loss, dysfunction and altered dynamics in Huntington's disease. *Hum Mol Genet* **19**:3919-3935 https://doi.org/10.1093/hmg/ddq306 | PubMed

Kim M., Lee H.S., LaForet G., McIntyre C., Martin E.J., Chang P., Kim T.W., Williams M., Reddy P.H., Tagle D., *et al.* (1999) Mutant huntingtin expression in clonal striatal cells: dissociation of inclusion formation and neuronal survival by caspase inhibition. *J Neurosci* **19**:964-973 https://doi.org/10.1523/jneurosci.19-03-00964.1999 | PubMed

Klumperman J (2011) Architecture of the mammalian Golgi. *Cold Spring Harb Perspect Biol* **3** https://doi.org/10.1101/cshperspect.a005181 | PubMed

Kordasiewicz H.B., Stanek L.M., Wancewicz E.V., Mazur C., McAlonis M.M., Pytel K.A., Artates J.W., Weiss A., Cheng S.H., Shihabuddin L.S., *et al.* (2012) Sustained therapeutic reversal of Huntington's disease by transient repression of huntingtin synthesis. *Neuron* **74**:1031-1044 https://doi.org/10.1016/j.neuron.2012.05.009 | PubMed

Lajoie P., Snapp E.L (2010) Formation and toxicity of soluble polyglutamine oligomers in living cells. *PLoS One* **5**:e15245 https://doi.org/10.1371/journal.pone.0015245 | PubMed

Lanciego J.L., Luquin N., Obeso J.A (2012) Functional neuroanatomy of the basal ganglia. *Cold Spring Harb Perspect Med* **2**:a009621 https://doi.org/10.1101/cshperspect.a009621 | PubMed

Lebon S., Bruneel A., Drunat S., Albert A., Csaba Z., Elmaleh M., Ntorkou A., Tenier Y., Fenaille F., Gressens P., *et al.* (2025) A biallelic variant in GORASP1 causes a novel Golgipathy with glycosylation and mitotic defects. *Life Sci Alliance* **8** https://doi.org/10.26508/lsa.202403065 | PubMed

Lee H., Fenster R.J., Pineda S.S., Gibbs W.S., Mohammadi S., Davila-Velderrain J., Garcia F.J., Therrien M., Novis H.S., Gao F., *et al.* (2020) Cell Type-Specific Transcriptomics Reveals that Mutant Huntingtin Leads to Mitochondrial RNA Release and Neuronal Innate Immune Activation. *Neuron* **107**:891 https://doi.org/10.1016/j.neuron.2020.06.021 | PubMed

Legleiter J., Mitchell E., Lotz G.P., Sapp E., Ng C., DiFiglia M., Thompson L.M., Muchowski P.J. (2010) Mutant huntingtin fragments form oligomers in a polyglutamine length-dependent manner in vitro and in vivo. *J Biol Chem* **285**:14777-14790 https://doi.org/10.1074/jbc.m109.093708 | PubMed

Liu C., Mei M., Li Q., Roboti P., Pang Q., Ying Z., Gao F., Lowe M., Bao S (2017) Loss of the golgin GM130 causes Golgi disruption, Purkinje neuron loss, and ataxia in mice. *Proc Natl Acad Sci U S A* **114**:346-351 https://doi.org/10.1073/pnas.1608576114 | PubMed

Liu J.Y., Huang Y., Li T., Jiang Z., Zeng L.W., Hu Z.P (2021) The role of the Golgi apparatus in disease (Review). *Int J Mol Med* **47** https://doi.org/10.3892/ijmm.2021.4871 | PubMed

Liu Y., Chen X., Ma Y., Song C., Ma J., Chen C., Su J., Ma L., Saiyin H (2024) Endogenous mutant Huntingtin alters the corticogenesis via lowering Golgi recruiting ARF1 in cortical organoid. *Mol Psychiatry* https://doi.org/10.1038/s41380-024-02562-0 | PubMed

Ma L., Hu B., Liu Y., Vermilyea S.C., Liu H., Gao L., Sun Y., Zhang X., Zhang S.C (2012) Human embryonic stem cell-derived GABA neurons correct locomotion deficits in quinolinic acid-lesioned mice. *Cell Stem Cell* **10**:455-464 https://doi.org/10.1016/j.stem.2012.01.021 | PubMed

Machiela E., Southwell A.L (2020) Biological Aging and the Cellular Pathogenesis of Huntington's Disease. *J Huntingtons Dis* **9**:115-128 https://doi.org/10.3233/jhd-200395 | PubMed

Martin D.D., Ladha S., Ehrnhoefer D.E., Hayden M.R (2015) Autophagy in Huntington disease and huntingtin in autophagy. *Trends Neurosci* **38**:26-35 https://doi.org/10.1016/j.tins.2014.09.003 | PubMed

Mehta S.R., Tom C.M., Wang Y., Bresee C., Rushton D., Mathkar P.P., Tang J., Mattis V.B (2018) Human Huntington's Disease iPSC-Derived Cortical Neurons Display Altered Transcriptomics, Morphology, and Maturation. *Cell Rep* **25**:1081-1096. https://doi.org/10.1016/j.celrep.2018.09.076 | PubMed

Milnerwood A.J., Cummings D.M., Dallerac G.M., Brown J.Y., Vatsavayai S.C., Hirst M.C., Rezaie P., Murphy K.P (2006) Early development of aberrant synaptic plasticity in a mouse model of Huntington's disease. *Hum Mol Genet* **15**:1690-1703 https://doi.org/10.1093/hmg/ddl092 | PubMed

Milnerwood A.J., Gladding C.M., Pouladi M.A., Kaufman A.M., Hines R.M., Boyd J.D., Ko R.W., Vasuta O.C., Graham R.K., Hayden M.R., *et al.* (2010) Early increase in extrasynaptic NMDA receptor signaling and expression contributes to phenotype onset in Huntington's disease mice. *Neuron* **65**:178-190 https://doi.org/10.1016/j.neuron.2010.01.008 | PubMed

Morlot S., Roux A (2013) Mechanics of dynamin-mediated membrane fission. *Annu Rev Biophys* **42**:629-649 https://doi.org/10.1146/annurev-biophys-050511-102247 | PubMed

Mukai H., Isagawa T., Goyama E., Tanaka S., Bence N.F., Tamura A., Ono Y., Kopito R.R (2005) Formation of morphologically similar globular aggregates from diverse aggregation-prone proteins in mammalian cells. *Proc Natl Acad Sci U S A* **102**:10887-10892 https://doi.org/10.1073/pnas.0409283102 | PubMed

Nagai T., Suzuki Y., Kiyohara H., Susa E., Kato T., Nagamine T., Hagiwara Y., Tamura S., Yabe T., Aizawa C., *et al.* (2001) Onjisaponins, from the root of Polygala tenuifolia Willdenow, as effective adjuvants for nasal influenza and diphtheria-pertussis-tetanus vaccines. *Vaccine* **19**:4824-4834 https://doi.org/10.1016/s0264-410x(01)00215-8 | PubMed

Olenick M.A., Holzbaur E.L.F (2019) Dynein activators and adaptors at a glance. *J Cell Sci* **132** https://doi.org/10.1242/jcs.227132 | PubMed

Owens G.E., New D.M., West A.P., Bjorkman P.J (2015) Anti-PolyQ Antibodies Recognize a Short PolyQ Stretch in Both Normal and Mutant Huntingtin Exon 1. *Journal of Molecular Biology* **427**:2507-2519 https://doi.org/10.1016/j.jmb.2015.05.023 | PubMed

Passemard S., Perez F., Colin-Lemesre E., Rasika S., Gressens P., El Ghouzzi V (2017) Golgi trafficking defects in postnatal microcephaly: The evidence for "Golgipathies". *Prog Neurobiol* **153**:46-63 https://doi.org/10.1016/j.pneurobio.2017.03.007 | PubMed

Peters P.J., Ning K., Palacios F., Boshans R.L., Kazantsev A., Thompson L.M., Woodman B., Bates G.P., D'Souza-Schorey C (2002) Arfaptin 2 regulates the aggregation of mutant huntingtin protein. *Nat Cell Biol* **4**:240-245 https://doi.org/10.1038/ncb761 | PubMed

Poirier M.A., Li H.L., Macosko J., Cai S.W., Amzel M., Ross C.A (2002) Huntingtin spheroids and protofibrils as precursors in polyglutamine fibrilization. *Journal of Biological Chemistry* **277**:41032-41037 https://doi.org/10.1074/jbc.m205809200 | PubMed

Rao S., Kirschen G.W., Szczurkowska J., Di Antonio A., Wang J., Ge S., Shelly M. (2018) Repositioning of Somatic Golgi Apparatus Is Essential for the Dendritic Establishment of Adult-Born Hippocampal Neurons. *J Neurosci* **38**:631-647 https://doi.org/10.1523/jneurosci.1217-17.2017 | PubMed

Ravichandran Y., Goud B., Manneville J.B (2020) The Golgi apparatus and cell polarity: Roles of the cytoskeleton, the Golgi matrix, and Golgi membranes. *Curr Opin Cell Biol* **62**:104-113 https://doi.org/10.1016/j.ceb.2019.10.003 | PubMed

Sakamoto M., Sasaki K., Sugie A., Nitta Y., Kimura T., Gursoy S., Cinleti T., Iai M., Sengoku T., Ogata K., *et al.* (2021) De novo ARF3 variants cause neurodevelopmental disorder with brain abnormality. *Hum Mol Genet* **31**:69-81 https://doi.org/10.1093/hmg/ddab224 | PubMed

Saudou F., Finkbeiner S., Devys D., Greenberg M.E (1998) Huntingtin acts in the nucleus to induce apoptosis but death does not correlate with the formation of intranuclear inclusions. *Cell* **95**:55-66 https://doi.org/10.1016/s0092-8674(00)81782-1 | PubMed

Saudou F., Humbert S (2016) The Biology of Huntingtin. *Neuron* **89**:910-926 https://doi.org/10.1016/j.neuron.2016.02.003 | PubMed

Scherzinger E., Sittler A., Schweiger K., Heiser V., Lurz R., Hasenbank R., Bates G.P., Lehrach H., Wanker E.E (1999) Self-assembly of polyglutamine-containing huntingtin fragments into amyloid-like fibrils: implications for Huntington's disease pathology. *Proc Natl Acad Sci U S A* **96**:4604-4609 https://doi.org/10.1073/pnas.96.8.4604 | PubMed

Shirasaki D.I., Greiner E.R., Al-Ramahi I., Gray M., Boontheung P., Geschwind D.H., Botas J., Coppola G., Horvath S., Loo J.A., *et al.* (2012) Network organization of the huntingtin proteomic interactome in mammalian brain. *Neuron* **75**:41-57 https://doi.org/10.1016/j.neuron.2012.05.024 | PubMed

Silvestroni A., Faull R.L., Strand A.D., Moller T (2009) Distinct neuroinflammatory profile in post-mortem human Huntington's disease. *Neuroreport* **20**:1098-1103 https://doi.org/10.1097/wnr.0b013e32832e34ee

Sivaramakrishnan S., Spink B.J., Sim A.Y., Doniach S., Spudich J.A (2008) Dynamic charge interactions create surprising rigidity in the ER/K alpha-helical protein motif. *Proc Natl Acad Sci U S A* **105**:13356-13361 https://doi.org/10.1073/pnas.0806256105 | PubMed

Tabrizi S.J., Flower M.D., Ross C.A., Wild E.J (2020) Huntington disease: new insights into molecular pathogenesis and therapeutic opportunities. *Nat Rev Neurol* **16**:529-546 https://doi.org/10.1038/s41582-020-0389-4 | PubMed

Takahashi T., Kikuchi S., Katada S., Nagai Y., Nishizawa M., Onodera O (2008) Soluble polyglutamine oligomers formed prior to inclusion body formation are cytotoxic. *Hum Mol Genet* **17**:345-356 https://doi.org/10.1093/hmg/ddm311 | PubMed

Tang C.C., Feigin A., Ma Y., Habeck C., Paulsen J.S., Leenders K.L., Teune L.K., van Oostrom J.C., Guttman M., Dhawan V., *et al.* (2013) Metabolic network as a progression biomarker of premanifest Huntington's disease. *J Clin Invest* **123**:4076-4088 https://doi.org/10.1172/jci69411 | PubMed

Tousley A., Iuliano M., Weisman E., Sapp E., Richardson H., Vodicka P., Alexander J., Aronin N., DiFiglia M., Kegel-Gleason K.B (2019) Huntingtin associates with the actin cytoskeleton and alpha-actinin isoforms to influence stimulus dependent morphology changes. *Plos One* **14** https://doi.org/10.1371/journal.pone.0212337 | PubMed

Truant R., Atwal R.S., Desmond C., Munsie L., Tran T (2008) Huntington's disease: revisiting the aggregation hypothesis in polyglutamine neurodegenerative diseases. *Febs J* **275**:4252-4262 https://doi.org/10.1111/j.1742-4658.2008.06561.x | PubMed

Walker F.O (2007a) Huntington's disease. *Lancet* **369**:218-228 https://doi.org/10.1016/s0140-6736(07)60111-1 | PubMed

Walker F.O. (2007b) Huntington's disease. *Semin Neurol* **27**:143-150 https://doi.org/10.1055/s-2007-971176 | PubMed

Wei J.H., Seemann J (2009) Mitotic division of the mammalian Golgi apparatus. *Semin Cell Dev Biol* **20**:810-816 https://doi.org/10.1016/j.semcdb.2009.03.010 | PubMed

Wu L.L., Zhou X.F (2009) Huntingtin associated protein 1 and its functions. *Cell Adh Migr* **3**:71-76 https://doi.org/10.4161/cam.3.1.7511 | PubMed

Yadav S., Linstedt A.D (2011) Golgi positioning. *Cold Spring Harb Perspect Biol* **3** https://doi.org/10.1101/cshperspect.a005322 | PubMed

Zeitlin S., Liu J.P., Chapman D.L., Papaioannou V.E., Efstratiadis A. (1995) Increased apoptosis and early embryonic lethality in mice nullizygous for the Huntington's disease gene homologue. *Nat Genet* **11**:155-163 https://doi.org/10.1038/ng1095-155 | PubMed

Ma L., et al. (2012) Human embryonic stem cell-derived GABA neurons correct locomotion deficits in quinolinic acid-lesioned mice. *Cell Stem Cell* **10**:455-464 https://doi.org/10.1016/j.stem.2012.01.021 | PubMed

Butler A., Hoffman P., Smibert P., Papalexi E., Satija R (2018) Integrating single-cell transcriptomic data across different conditions, technologies, and species. *Nature Biotechnology* **36**:411 https://doi.org/10.1038/nbt.4096 | PubMed

Korsunsky I., et al. (2019) Fast, sensitive and accurate integration of single-cell data with Harmony. *Nature Methods* **16**:1289 https://doi.org/10.1038/s41592-019-0619-0 | PubMed

Zhou Y. Y., et al. (2019) Metascape provides a biologist-oriented resource for the analysis of systems-level datasets. *Nat Commun* **10** https://doi.org/10.1038/s41467-019-09234-6 | PubMed

van de Sande B., et al. (2020) A scalable SCENIC workflow for single-cell gene regulatory network analysis. *Nature Protocols* **15**:2247-2276 https://doi.org/10.1038/s41596-020-0336-2 | PubMed

Peer reviews

Reviewer #1 (Public review):

Summary:

The authors aim to characterize Huntingtin (HTT) aggregates in various cells and tissues and propose that mutant polyQ HTT (mHTT) assembles at the Golgi apparatus, thereby impairing Golgi organization and function. They further suggest that such Golgi defects might contribute to disease pathology, including neurodegeneration.

Strengths:

The study spans a wide range of disciplines, including genetics, cell biology, neuroscience, and systems biology, and employs diverse methodologies such as iPSC, 3D SIM microscopy, omics approaches, organoid culture, electrophysiology, and antisense depletion.

Weaknesses:

While the breadth of techniques is impressive, the central premise of the work-the structural and functional relationship between polyQ assemblies and the Golgi apparatus-is not supported by sufficiently rigorous cell biological evidence.

A major concern is that much of the cell biology data remains descriptive and lacks mechanistic depth. The findings are fragmented and not integrated into a coherent molecular or cellular model. Instead of building a logical progression of experiments, the study presents a collection of observations that appear disconnected and, at times, driven more by technical capability than by hypothesis-driven design.

Critically, the key claim that polyQ HTT functionally disrupts the Golgi (Golgipathy) is not convincingly demonstrated. Many observations could be more simply explained by the polyQ HTT localization to the Golgi and known Golgi sensitivities to perturbations (e.g., starvation or Brefeldin A treatment), rather than by a specific mechanistic role of polyQ HTT.

The manuscript also suffers from issues in organization and clarity, including imprecise descriptions and figures that are difficult to interpret.

Major Concerns:

(1) Golgi localization

The localization of polyQ HTT relies entirely on the antibody 3B5H10, which is foundational to the study. However, previous reports using the same antibody have described predominantly cytosolic localization. This discrepancy must be addressed rigorously by independent validation using alternative antibodies or tagged, exogenously expressed polyQ HTT constructs that should be shown to colocalize with 3B5H10 signals.

Furthermore, the Golgi is identified solely using GM130, a cis-Golgi and ER exit site marker. This raises ambiguity: does polyQ HTT associate with the entire Golgi or only recruit GM130? Could the observed signal correspond to a sub-Golgi compartment?

If polyQ HTT is indeed Golgi-associated, several key observations become expected rather than novel. For example, in Figure 4I-M, sensitivity to Brefeldin A is unsurprising, as Golgi structure collapses upon such treatment; in Figure 4N-O, co-fragmentation with the Golgi is expected under Golgi-disrupting conditions.

(2) 3D rendering

The extensive use of 3D rendering appears unnecessary and, in some cases, misleading. The rendered images do not provide additional insight beyond conventional 2D fluorescence images. Serial 2D fluorescence sections should be more objective in representing the 3D organization. In Figure 2A and Figure 5A, red line features in 3D beige polyQ HTT structures resemble unrelated biological structures, such as vasculature, which is inappropriate.

There is also an inconsistency in rendering. For example, fine mesh-like structures are shown in some figures (e.g., Figure 2A, Figure 4A), whereas others appear as amorphous aggregates (e.g., Figure 5A, Figure S2B), without explanation.

(3) Quantification of area and volume

The manuscript extensively quantifies the area and volume of polyQ assemblies (e.g., Figure 2B, C and Figure 3B, C, E, G, H). These measurements are not reliable. First, the structures appear filamentous and likely below the diffraction limit. Second, fluorescence signals are broadened by the point spread function (PSF), artificially inflating measured dimensions. Last, even with 3D SIM (~100 nm resolution), fine structural details remain unresolved. Thus, these quantitative measurements lack physical meaning and might not be used to support conclusions.

(4) Interpretation of structural features (Figure 2A)

Descriptions such as "parallel spindles" and "ring-like assemblies" are not clearly supported by the data. The terminology is ambiguous, and the claimed structures are not discernible. The use of the term "interaction" with the nuclear membrane is also inappropriate. At best, the data suggest colocalization, which itself is not convincingly demonstrated.

(5) Mitotic fragmentation (Figure 2E)

The conclusion that polyQ assemblies fragment during mitosis lacks proper controls. It is unclear whether these cells exhibited intact "fabric-like" assemblies during interphase, or the observed structures were already fragmented prior to mitosis.

(6) Fixation-induced fragmentation (Figure 2F)

The claim that fixation-induced fragmentation reflects a unique dynamic property of polyQ assemblies is likely an overinterpretation. This phenomenon may simply represent a fixation artifact. Therefore, it cannot be used as evidence for in-cellulo structural dynamics.

(7) Nuclear localization claims (Figure 5A)

The assertion that polyQ assemblies "almost completely occupy the nucleus" is not supported. The images are more consistent with perinuclear localization, typical of the Golgi region. There is no clear evidence for nucleoplasmic distribution.

(8) Drug treatment and data interpretation (Figure 3D-E)

The x-axis in Figure 3E is non-linear, which is inappropriate unless explicitly justified. Furthermore, the rationale for using Onjisaponin F is unclear. What is its known mechanism? Does it affect Golgi organization? Without this context, observed effects may reflect Golgi perturbation rather than specific effects on polyQ assemblies.

https://doi.org/10.7554/eLife.111495.1.sa2

Reviewer #2 (Public review):

Summary:

In this study, the authors report the hitherto unobserved types of HTT assemblies observed in human fibroblasts and iPCS-derived neurons in 2D and 3D culture, applying a state-of-the-art confocal microscopy imaging with near 64 nm resolution to decode their structures. They further demonstrate that these assemblies closely contact with various types of Golgi ribbons, stacks, vesicles, and Golgi-derived clathrin-coated vesicles but not mitochondria. They also used single-cell RNAseq to show some interesting findings that supported the suggested defects in Golgi-related function, specifically by downregulation of various cellular processes related to Golgi and vesicle transport functions. They also replicate mHTT nuclear accumulations in striatal neurons, which is considered to be a hallmark of HD pathology, by using long-term neuronal culture. Furthermore, the assemblies showed differential responses to glucose starvation and to autophagy enhancer treatment by onjisaponin F for mutant HTT assemblies, but not for the healthy siblings, in fibroblasts and neurons. Onjisaponin F treatment did not reverse nuclear deposition. They also showed that ASO shortens these polyQ assemblies but does not change neuronal firings that are detected by HD-MEA. Notably, they also used human brain samples to show the existence of polyQ assemblies in fetal and child brain samples. This part is impressive.

Overall, this work reports a novel polyQ assembly, which was previously reported as a pathogenic factor, has not been reported before for HTT, is related to Golgi activities and vesicular transport, and is dismantled in HD patient cells. The intensive immunostaining and super-resolution scanning are impressive and definitely strengthened by the impact of the findings. The scRNAseq data adds another layer to the observed Golgi impairments and their suggested relationship to Golgi function. The drug testing for polyQ assemblies, especially polyQ assemblies in HD cells, is preliminary. However, the data in this study are enough to support the existence of polyQ assemblies in human cells and their specific relationships with the Golgi apparatus.

Strengths:

In this study, the authors used the cells from a large HD family and fetal/child brain samples to decode the structure of endogenous polyQ assemblies. This part is impressive. The intensive staining and super-resolution scanning are amazing. The spatial relationships of polyQ assemblies with the Golgi apparatus and mitochondria are well illustrated.

Weaknesses:

Although they used healthy sibling cells as a control, an isogenic control (genetic correction of the mutant gene) is lacking. Based on the Golgipathy of mHTT, they did a drug screening. The

drug testing for polyQ assemblies is preliminary. More rigorous validation, such as scRNA seq and proteomic analysis, etc., is necessary to reach a systemic conclusion.

https://doi.org/10.7554/eLife.111495.1.sa1

Author response:

> ***Reviewer #1 (Public review):***
>
> *Weaknesses:*
>
> *While the breadth of techniques is impressive, the central premise of the work-the structural and functional relationship between polyQ assemblies and the Golgi apparatus-is not supported by sufficiently rigorous cell biological evidence.*
>
> *A major concern is that much of the cell biology data remains descriptive and lacks mechanistic depth. The findings are fragmented and not integrated into a coherent molecular or cellular model. Instead of building a logical progression of experiments, the study presents a collection of observations that appear disconnected and, at times, driven more by technical capability than by hypothesis-driven design.*
>
> *Critically, the key claim that polyQ HTT functionally disrupts the Golgi (Golgipathy) is not convincingly demonstrated. Many observations could be more simply explained by the polyQ HTT localization to the Golgi and known Golgi sensitivities to perturbations (e.g., starvation or Brefeldin A treatment), rather than by a specific mechanistic role of polyQ HTT.*
>
> *The manuscript also suffers from issues in organization and clarity, including imprecise descriptions and figures that are difficult to interpret.*

We thank the Reviewer for their time, valuable comments, and recognition of our technical expertise and resources. With our specialized background in pathology and super-resolution microscopy, our research heavily relies on structurally precise histological methods to address these fundamental biological questions. Furthermore, our laboratory maintains one of the largest repositories of patient-derived and healthy control fibroblasts, as well as iPSC lines, within the Huntington's disease (HD) research community. Because these patient-derived and engineered cell models express endogenous mutant HTT (mHTT) within an authentic genetic background, they provide a uniquely powerful system for decoding HD pathogenesis.

We appreciate the Reviewer's comment regarding hypothesis-driven design. Classically, a hypothesis-driven approach relies on well-established, highly stable experimental platforms. However, a key finding of our study is the highly fragile and volatile nature of polyQ assemblies, particularly when subjected to post-fixation and oxidative stress. Because these structures can behave unpredictably under stress, we utilized an unbiased, data-driven approach leveraging our high-resolution imaging pipeline to explore polyQ assemblies in both healthy and HD cells.

Importantly, hypothesis-driven and data-driven methods are complementary rather than mutually exclusive. For instance, if a real-time tracking method were developed to endogenously label native HTT in living cells, it would open the door for direct hypothesis testing regarding polyQ assembly mechanics. Despite the current technical limitations of the field, our study successfully overcomes these challenges to reveal the spatial tomography and unique dynamics of polyQ assemblies directly within patient-derived cells. We fully discussed the limitations of this research in the discussion section.

We appreciate the Reviewer's critical assessment regarding the functional disruption of the Golgi apparatus (Golgipathy). To rigorously investigate this phenomenon, we employed a comprehensive suite of methodologies ranging from live-cell imaging to single-cell RNA sequencing. Our findings build directly upon a well-established body of literature. We previously demonstrated that mutant huntingtin (mHTT) disrupts Golgi function within the neural tubes of human cortical organoids (hCO) (Liu et al., 2024), aligning with broader neurodevelopmental defects observed in HD (Barnat et al., 2020). Furthermore, prior independent studies have confirmed that both HTT knockdown and the presence of mHTT impair Golgi-to-plasma membrane trafficking, notably in primary fibroblasts from homozygous $Htt^{140Q/140Q}$ knock-in mice (Brandstaetter et al., 2014); mHTT also affects post-Golgi trafficking of proteins (del Toro et al., 2006). Backed by this literary consensus and our own multi-modal data, which Reviewer 2 also noted as sufficient, we are confident that our manuscript provides a robust, multi-layered demonstration of mHTT-induced Golgipathy.

In this study, we found that polyQ assemblies and the Golgi form a Golgi-polyQ complex mediated by ARF1 and ARFIP2. Thus, the structural coupling of polyQ assemblies with the Golgi apparatus under starvation, during the cell cycle, is rational.

Based on the reviewer suggestion, we will completely revise the entire manuscript. Hopefully, this revision will meet the requirement of smoothness and clarity.

> *Major Concerns:*
>
> *(1) Golgi localization*
>
> *The localization of polyQ HTT relies entirely on the antibody 3B5H10, which is foundational to the study. However, previous reports using the same antibody have described predominantly cytosolic localization. This discrepancy must be addressed rigorously by independent validation using alternative antibodies or tagged, exogenously expressed polyQ HTT constructs that should be shown to colocalize with 3B5H10 signals.*

Despite historical inconsistencies across existing publications (Barnat et al., 2020; Hickman et al., 2022; Shen et al., 2019; Tousley et al., 2019), we noticed that the immunostaining results of multiple HTT antibodies are consistent with our data (DiFiglia et al., 1995; Ko et al., 2001; Velier et al., 1998; Wheeler et al., 2000). Although these pioneering studies lacked modern 3D high-resolution imaging and standardized staining protocols, their reported 2D distribution patterns heavily resemble our results. For instance, transmission electron microscopy (TEM) immunolabeling originally revealed that HTT localizes along Golgi cisternae (DiFiglia et al., 1995) and formed organized and parallel fibrils (DiFiglia et al., 1997). Furthermore, immunostaining with a panel of distinct antibodies, including MV2, 3, 4, 5, 6, and 1F8, demonstrated characteristic Golgi-like distribution patterns for HTT (Ko et al., 2001). In addition, our polyQ antibody immunostaining in human fetal brain, which is reflective of polyQ assembly, is nearly identical to the staining results of Barnat et al., publication in Science (Barnat et al., 2020).

We have carefully checked two early publications, which reported that 3B5H10 only binds expanded polyQ but does not bind a normal polyQ (non-disease causing), which displays a part of a neuron that has a cytosolic diffuse pattern of HTT in 3B5H10 staining (Legleiter et al., 2009; Miller et al., 2011). Based on our extensive experience with HTT immunohistochemistry, we hypothesize that this diffuse signal may reflect nonspecific background artifacts, often caused by high antibody concentrations, poor tissue fixation, inadequate post-incubation washing, or the presence of effete cells, or premature fragmentation of the polyQ tract prior to staining. Interestingly, Miller et al. utilized a rapid tissue-perfusion and sectioning protocol originally published in Brain Research Bulletin (Ko et al., 2001), which is optimized to preserve intact polyQ assemblies. When reviewing the

original Brain Research Bulletin study (Ko et al., 2001), we noted that the immunostaining profiles for polyQ-containing HTT peptides (specifically using antibodies MW2, MW3, MW4, MW5, and 1F8) are entirely consistent with our data, yet completely diverge from the patterns reported by the Muchowski group (Legleiter et al., 2009; Miller et al., 2011) (please see Ko et al., 2001.Legleiter et al., 2009; Miller et al., 2011). Furthermore, contrary to the Muchowski group's claims, subsequent biophysical evidence by Owens et al. (2015) independently confirmed that 3B5H10 binds to both normal and expanded polyQ sequences in huntingtin exon 1 fusion proteins (Owens et al., 2015). Together, these observations strongly support the validity of our staining profiles.

Several antibodies, including MV1, 1C2, and 3B5H10, were previously reported to recognize the expanded, pathogenic polyQ tracts of HTT (Khoshnan et al., 2002; Miller et al., 2011; Wang et al., 2008). However, emerging studies reveal that these antibodies actually bind both short and long polyQ sequences (Klein et al., 2013; Owens et al., 2015). Because a standard antibody Fab epitode typically spans only 5 to 15 amino acids (or 3 to 4 sugar residues), and normal HTT polyQ repeats range from 18 to 24, it is theoretically impossible for an antibody to exclusively target expanded polyQ while sparing normal polyQ.

We previously noticed that 3B5H10 antibody immunostaining signals are located in the long projection of striatal neurons. As we did not notice an intact neuron in the two publications, we have no idea about the 3B5H10 antibody signals in the neuronal projections of those images.

We investigated whether the polyQ assemblies detected by the 3B5H10 antibody contain full-length or large fragments of huntingtin (HTT). To test this, we selected two distinct HTT antibodies: EM48, which binds the first 256 amino acids (excluding the polyQ stretch), and 3E10, which targets the HDA region (amino acids 1171–1177). In patient fibroblasts, the immunostaining patterns for both EM48 and 3E10 were nearly identical to those observed with 3B5H10. These results demonstrate that the polyQ assemblies in fibroblasts are primarily composed of HTT proteins (see Author response image 1). We will include the results of EM48 and 3E10 immunostaining in the revised version.

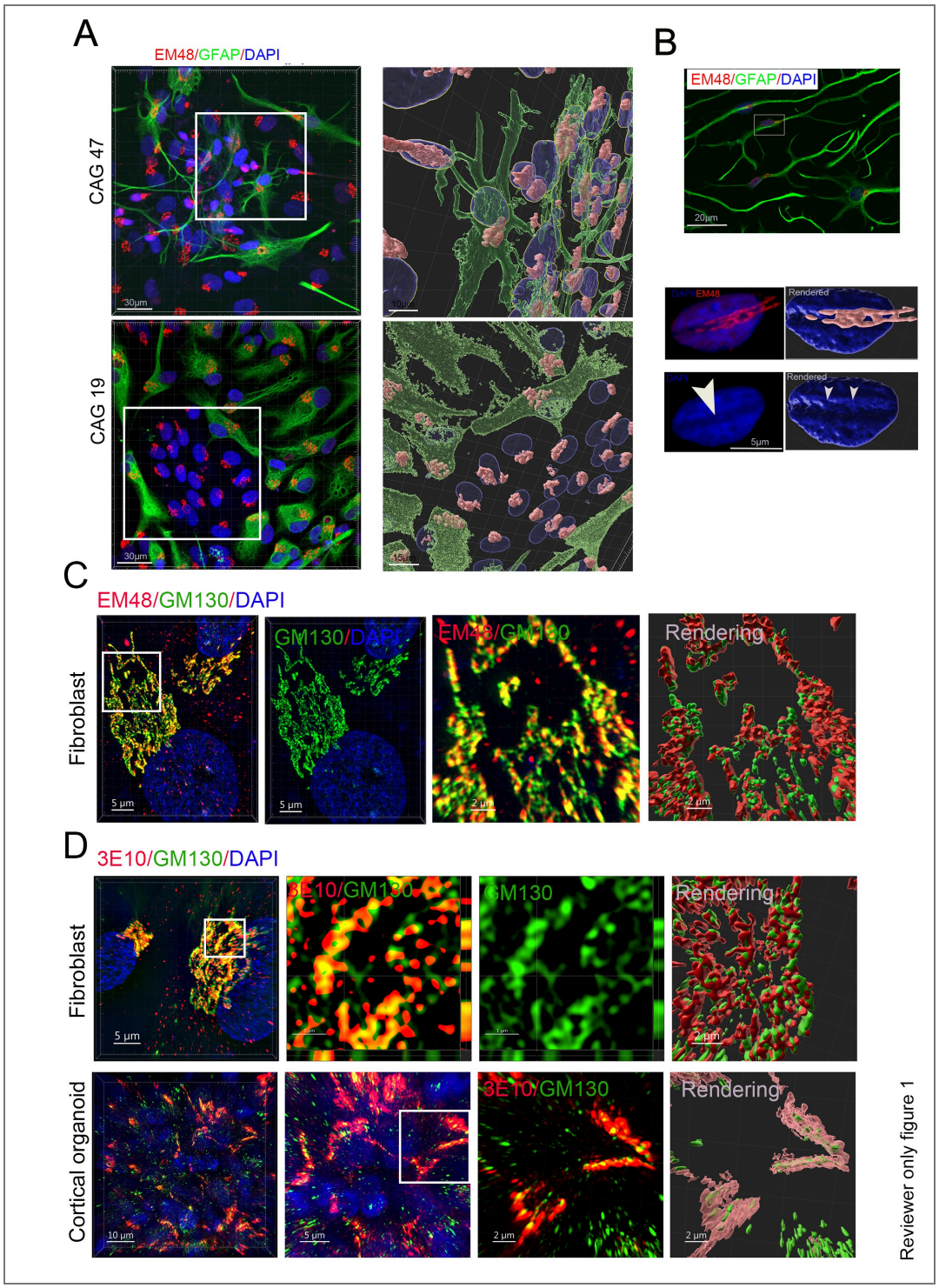

Author response image 1. (A) GFAP and EM48 antibodies staining of the astrocytes derived from HD patient and healthy sibling iPSCs showed polyQ assembly in the astrocytes derived from iPSC. (B). The spindle of polyQ assembly formed a dent on the nuclear surface of astrocytes. (C, D) Coimmunostaining of GM130 antibody with 3E10 or EM48 antibody in fibrobalsts revealed that polyQ assemblies contain great amount of HTTs. The middle and right panel are the sectional view boxed region (D) and the boxed region are a magnified part or rendering part (C, D) .

We also check whether the transfected exogenous HTT fragment of the first exon can be recruited into polyQ assemblies. We transfected fibroblasts with three vectors of the HTT first exon containing 19, 23, and 74 CAGs, respectively. The exogenous HTT fragments of the first

exon did not significantly recruit into endogenous polyQ assemblies-Golgi complexes of fibroblasts (please refer to Reviewer only figure 5). We will include this part in the revised version.

In the cover letter, we told the editor that we have been studying this structure for over ten years. The results have been stable for over ten years.

> *Furthermore, the Golgi is identified solely using GM130, a cis-Golgi and ER exit site marker. This raises ambiguity: does polyQ HTT associate with the entire Golgi or only recruit GM130? Could the observed signal correspond to a sub-Golgi compartment?*

Thank you for highlighting the precise sub-Golgi localization of GM130 as resolved by electron microscopy. We agree that transmission electron microscopy (TEM) demonstrates GM130 is restricted to the cis-Golgi network, intercisternal regions, and tubular structures, and is absent from the trans-Golgi (Nakamura et al., 1995). Given that individual Golgi cisternae measure approximately 20 nm in width, resolving cis- versus trans-Golgi sub-compartments exceeds the physical resolution limits of our microscopy system. Consequently, GM130 was utilized here as a robust, widely accepted pan-Golgi marker rather than a tool for sub-compartmental differentiation. To specifically evaluate the trans-Golgi network (TGN), we tracked Clathrin+ vesicles, which actively sort at the TGN (Klumperman, 2011). Our Clathrin staining confirms that polyQ assemblies localize to both the cis- and trans-Golgi compartments, as clearly demonstrated in the new lateral view projections provided in revised Figure 4C.

> *If polyQ HTT is indeed Golgi-associated, several key observations become expected rather than novel. For example, in Figure 4I-M, sensitivity to Brefeldin A is unsurprising, as Golgi structure collapses upon such treatment; in Figure 4N-O, co-fragmentation with the Golgi is expected under Golgi-disrupting conditions.*

We agree that our data demonstrate the formation of a functionally coupled polyQ assembly–Golgi complex. Physically and structurally, the dynamics of polyQ assemblies are intrinsically linked to Golgi dynamics under distinct physiological states, including cell cycle progression and energy deprivation. This structural coupling is mediated by ADP-ribosylation factor 1 (ARF1). Specifically, the polyQ tract of HTT interacts with ARFIP2, which is one of the key effector proteins that physically bind active ARF1. Mechanistically, ARF1 is recruited to the Golgi membrane upon GDP-to-GTP exchange catalyzed by guanine nucleotide-exchange factors (GEFs). Consequently, treatment with Brefeldin A (BFA)—which inhibits ARF1 activation—effectively decouples the polyQ assemblies from both intact and fragmented Golgi structures.

Regarding the question of novelty, we define experimental novelty based on generating entirely unprecedented, empirical data that either confirms or redefines biological expectations, rather than evaluating conceptual expectations themselves. We believe the uncovering of this real-time, stimulus-responsive coupling mechanism provides fundamentally novel insights into HTT biology.

> *(2) 3D rendering*
>
> *The extensive use of 3D rendering appears unnecessary and, in some cases, misleading. The rendered images do not provide additional insight beyond conventional 2D fluorescence images. Serial 2D fluorescence sections should be more objective in representing the 3D organization.*

Thanks for pointing out the 3D rendering. While 3D rendering provides an essential spatial approximation of fluorescently labeled architectures, it offers significantly more precise structural information than conventional 2D or serial section imaging alone (Cao et al., 2023; Han et al., 2021; Hexige et al., 2015). A primary objective of our study was to evaluate these

subcellular features within their intact, native three-dimensional context rather than relying solely on two-dimensional cross-sections. Crucially, without complete volumetric rendering, it is mathematically and visually challenging to accurately delineate complex morphological features, such as the nuclear gorge or true intranuclear accumulation. Consequently, 3D volumetric analysis and rendering are entirely indispensable for the accurate interpretation of the structural data presented in this study.

> *In Figure 2A and Figure 5A, red line features in 3D beige polyQ HTT structures resemble unrelated biological structures, such as vasculature, which is inappropriate.*

We would like to clarify that there is no vasculature present within the referenced 3D rendering. The features the reviewer is highlighting are artifacts of the pseudo-coloring used exclusively to mask and visualize the surface tomography. In volumetric 3D rendering, pseudo-colors are assigned strictly to enhance visual clarity and contrast for the reader; they carry no intrinsic biological meaning or cellular identity. Furthermore, from a structural standpoint, the narrow red features in the rendered image are orders of magnitude smaller than true microvasculature. Functional microvessels possess a minimum diameter of 6 to 45 micrometers and exhibit a defined vascular lumen, endothelial cells, a basement membrane, pericytes, and a tunica intima. Therefore, based on both the scale of the image and established histological criteria, these features cannot biologically or structurally represent vasculature.

> *There is also an inconsistency in rendering. For example, fine mesh-like structures are shown in some figures (e.g., Figure 2A, Figure 4A), whereas others appear as amorphous aggregates (e.g., Figure 5A, Figure S2B), without explanation.*

The selection of opacity and color masks in our 3D volumetric reconstructions is systematically chosen to optimize the visual clarity and spatial relationships between intersecting sub-cellular structures. For example, as shown in the fourth and fifth panels, an opaque blue mask was applied to clearly define the outer surface tomography. Conversely, in the third panel, a semi-transparent blue mask was utilized for the nucleus. This transparency is methodologically necessary because a subset of polyQ fragments is embedded within or localized directly inside the nuclear envelope; a transparent mask allows for the unambiguous visualization of these internal structures. Similarly, the inset in Figure 5A illustrates the distinct intranuclear occupancy pattern of polyQ, which also necessitates a transparent nuclear boundary. Collectively, these volumetric rendering strategies provide critical spatial and structural depth that cannot be captured by conventional 2D cross-sections or unconstructed serial imaging.

> *(3) Quantification of area and volume*
>
> *The manuscript extensively quantifies the area and volume of polyQ assemblies (e.g., Figure 2B, C and Figure 3B, C, E, G, H). These measurements are not reliable. First, the structures appear filamentous and likely below the diffraction limit. Second, fluorescence signals are broadened by the point spread function (PSF), artificially inflating measured dimensions. Last, even with 3D SIM (~100 nm resolution), fine structural details remain unresolved. Thus, these quantitative measurements lack physical meaning and might not be used to support conclusions.*

We appreciate the reviewer's thoughtful critique regarding the quantification of area and volume. Our measurements are derived from immunofluorescent signals captured via structured illumination microscopy (SIM) and confocal imaging. If the reviewer's concern is that antibody-labeled structures do not perfectly match the absolute physical dimensions of native polyQ assemblies due to the linkage error of the primary-secondary antibody complex, we agree conceptually.

However, our imaging pipeline is optimized to minimize these discrepancies. Our SIM resolution reaches approximately 64 nm. Given that the total observed thickness of the fluorophore-labeled polyQ assemblies exceeds 200 nm, these structures reside well within the detectable range of our super-resolution system, minimizing diffraction-induced overestimation. Regarding the point spread function (PSF) and optical distortion, we emphasize that all comparative quantifications across experimental groups were conducted under identical imaging parameters and thresholds, ensuring a standardized baseline. Furthermore, our acquisition systems (Leica, Nikon, and Zeiss) utilize advanced deconvolution algorithms specifically designed to mitigate PSF-related blur. While we observed that deconvolution yielded negligible baseline improvements when using high-numerical-aperture objectives (63x) or 100x, oil immersion), it validates that our raw high-resolution scanning was already highly optimized.

We acknowledge that an immunolabeled complex is not structurally identical to a naked, pure polyQ tract. Nonetheless, indirect immunofluorescence remains the most robust method to evaluate spatial distribution in situ. Indeed, cryo-EM studies have highlighted that native polyQ tracts are highly flexible and structurally dynamic, making them exceptionally difficult to resolve in their native state (Guo et al., 2018). Intriguingly, we observed that antibody-bound polyQ assemblies remain structurally stable for several weeks with minimal fragmentation, suggesting that antibody binding may structurally stabilize these highly flexible regions. Consequently, indirect immunolabeling provides an indispensable framework for capturing these assemblies within the cellular environment.

> *(4) Interpretation of structural features (Figure 2A)*
>
> *Descriptions such as "parallel spindles" and "ring-like assemblies" are not clearly supported by the data. The terminology is ambiguous, and the claimed structures are not discernible. The use of the term "interaction" with the nuclear membrane is also inappropriate. At best, the data suggest colocalization, which itself is not convincingly demonstrated.*

Please refer to Fig. 2A (middle upper), Fig. 2F, and Fig. 4C for “parallel spindles”. Please refer to Fig. 5I, J, and Fig.S3C (right panel) for additional clear “ring-like assemblies”. Due to the unique spatial distribution of the 'ring-like assemblies', observing multiple rings within a single spindle is technically challenging. Accordingly, we have tempered our statement in the revised manuscript to accurately reflect this limitation. Furthermore, it is important to note that the visualized structures represent the fluorescent signal from secondary antibodies rather than direct imaging of the proteins themselves. Consequently, we cannot definitively confirm whether this immunostaining pattern precisely replicates the native state of polyQ assemblies within the cellular environment.

> *(5) Mitotic fragmentation (Figure 2E)*
>
> *The conclusion that polyQ assemblies fragment during mitosis lacks proper controls. It is unclear whether these cells exhibited intact "fabric-like" assemblies during interphase, or the observed structures were already fragmented prior to mitosis.*

We thought that we had displayed enough non-mitotic cells in this study (Fig. 2A, D, Fig. 4A, F). Most of the cells in this study are non-mitotic cells (G1+S+G2). Thus, we consider the control of non-mitotic cells to be redundant here.

> *(6) Fixation-induced fragmentation (Figure 2F)*
>
> *The claim that fixation-induced fragmentation reflects a unique dynamic property of polyQ assemblies is likely an overinterpretation. This phenomenon may simply represent*

> *a fixation artifact. Therefore, it cannot be used as evidence for in-cellulo structural dynamics.*

By definition, a laboratory artifact refers to any unintended structural detail, distortion, or error introduced by experimental equipment or the preparation process. We contend that the observed phenomenon represents a native chemical characteristic of the HTT polyQ domain inside cells following paraformaldehyde (PFA) fixation, rather than a technical artifact. Similar structural features have been documented by other investigators in tissue samples (Ferrante et al., 1997). A classic textbook example of an artifact is the lamina lucida of the basal lamina, which is artificially generated during electron microscopy tissue processing and does not exist in living tissue. In contrast, the fragmentation of polyQ assemblies occurs naturally both in living cells subjected to stress and during post-fixation processing.

> *(7) Nuclear localization claims (Figure 5A)*
>
> *The assertion that polyQ assemblies "almost completely occupy the nucleus" is not supported. The images are more consistent with perinuclear localization, typical of the Golgi region. There is no clear evidence for nucleoplasmic distribution.*

Please refer to the rendering image in the upper left inner insert of HD neurons (the blue [transparent] is the nucleus and the pink white is polyQ). The almost complete occupation of the nucleus is crystal clear in these images (rendered inner inserts, upper left). In iPSC-induced HD neurons, it is not only distributed in the nucleus but also in the cytoplasm. Based on your description, you might refer to the cytoplasmic polyQ assemblies but not the nucleus in the rendering image of the upper left (left panel). We will add a label in the revised version for clarity (white arrows for nuclear accumulation). In this manuscript, we have enough figures that clearly show the nuclear accumulation. Please also refer to Fig. 7 and Fig. S2 for additional images of nuclear accumulation.

> *(8) Drug treatment and data interpretation (Figure 3D-E)*
>
> *The x-axis in Figure 3E is non-linear, which is inappropriate unless explicitly justified. Furthermore, the rationale for using Onjisaponin F is unclear. What is its known mechanism? Does it affect the Golgi organization? Without this context, observed effects may reflect Golgi perturbation rather than specific effects on polyQ assemblies.*

We appreciate the reviewer pointing out Figure 3E. In this experiment, Huntington's disease (HD) fibroblasts were cultured in a low-glucose medium for the first 72 hours, which accounts for the linear trend observed across the first four data points. Following this 72-hour period, the cells were switched to a high-glucose medium and cultured for an additional 48 hours to evaluate subsequent dynamic changes in the polyQ assemblies. To improve visual clarity, we have color-coded these distinct treatment conditions in the revised manuscript, using red to denote low-glucose treatment and green to denote high-glucose treatment.

Regarding the choice of Onjisaponin treatment (a concern also raised by another reviewer), Onjisaponin is an active component derived from Radix Polygalae (Yuan Zhi). Previous literature indicates that Onjisaponin B enhances autophagy, accelerates the degradation of mutant α-synuclein and huntingtin in vitro, and activates the AMPK-mTOR signaling pathway (Wu et al., 2013). To optimize our experimental model, we screened multiple variants—specifically Onjisaponin B, D, and F. We determined that Onjisaponin F exhibits remarkably low cytotoxicity while maintaining a robust autophagy-enhancing capacity in both human fibroblasts and iPSC-derived neurons. Consequently, Onjisaponin F was selected for our human cell line experiments (please refer to the Reviewer only image 3). While we did not previously assess Golgi apparatus alterations under Onjisaponin F treatment, we recognize the value of this metric. We are currently evaluating changes to both the Golgi apparatus and neuronal firing rates following Onjisaponin F exposure, and this new dataset will be integrated into our revision.

> ***Reviewer #2 (Public review):***
>
> *[...] Overall, this work reports a novel polyQ assembly, which was previously reported as a pathogenic factor, has not been reported before for HTT, is related to Golgi activities and vesicular transport, and is dismantled in HD patient cells. The intensive immunostaining and super-resolution scanning are impressive and definitely strengthened by the impact of the findings. The scRNAseq data adds another layer to the observed Golgi impairments and their suggested relationship to Golgi function. The drug testing for polyQ assemblies, especially polyQ assemblies in HD cells, is preliminary. However, the data in this study are enough to support the existence of polyQ assemblies in human cells and their specific relationships with the Golgi apparatus.*

We sincerely thank the reviewer for their time, dedication, and insightful evaluation of our manuscript. We agree that the drug screening component represents an initial phase of discovery, and we appreciate the opportunity to clarify this in our text. As the reviewer notes, executing high-throughput or exhaustive drug screenings in human brain organoids is exceptionally resource- and time-intensive due to prolonged culture requirements. We will provide more mechanistic and physiological details of these drug in the future.

> *Strengths:*
>
> *In this study, the authors used the cells from a large HD family and fetal/child brain samples to decode the structure of endogenous polyQ assemblies. This part is impressive. The intensive staining and super-resolution scanning are amazing. The spatial relationships of polyQ assemblies with the Golgi apparatus and mitochondria are well illustrated.*
>
> *Weaknesses:*
>
> *Although they used healthy sibling cells as a control, an isogenic control (genetic correction of the mutant gene) is lacking. Based on the Golgipathy of mHTT, they did a drug screening. The drug testing for polyQ assemblies is preliminary. More rigorous validation, such as scRNA seq and proteomic analysis, etc., is necessary to reach a systemic conclusion.*

References

Barnat, M., Capizzi, M., Aparicio, E., Boluda, S., Wennagel, D., Kacher, R., Kassem, R., Lenoir, S., Agasse, F., Braz, B.Y., et al. (2020). Huntington's disease alters human neurodevelopment. Science 369, 787-793.

Brandstaetter, H., Kruppa, A.J., and Buss, F. (2014). Huntingtin is required for ER-to-Golgi transport and for secretory vesicle fusion at the plasma membrane. Dis Model Mech 7, 1335-1340.

Cao, L., Ma, L., Zhao, J., Wang, X., Fang, X., Li, W., Qi, Y., Tang, Y., Liu, J., Peng, S., et al. (2023). An unexpected role of neutrophils in clearing apoptotic hepatocytes in vivo. Elife 12.

del Toro, D., Canals, J.M., Gines, S., Kojima, M., Egea, G., and Alberch, J. (2006). Mutant huntingtin impairs the post-Golgi trafficking of brain-derived neurotrophic factor but not its Val66Met polymorphism. J Neurosci 26, 12748-12757.

DiFiglia, M., Sapp, E., Chase, K., Schwarz, C., Meloni, A., Young, C., Martin, E., Vonsattel, J.P., Carraway, R., Reeves, S.A., et al. (1995). Huntingtin is a cytoplasmic protein associated with vesicles in human and rat brain neurons. Neuron 14, 1075-1081.

DiFiglia, M., Sapp, E., Chase, K.O., Davies, S.W., Bates, G.P., Vonsattel, J.P., and Aronin, N. (1997). Aggregation of huntingtin in neuronal intranuclear inclusions and dystrophic neurites in brain. Science 277, 1990-1993.

Ferrante, R.J., Gutekunst, C.A., Persichetti, F., McNeil, S.M., Kowall, N.W., Gusella, J.F., MacDonald, M.E., Beal, M.F., and Hersch, S.M. (1997). Heterogeneous topographic and cellular distribution of huntingtin expression in the normal human neostriatum. J Neurosci 17, 3052-3063.

Guo, Q., Bin, H., Cheng, J., Seefelder, M., Engler, T., Pfeifer, G., Oeckl, P., Otto, M., Moser, F., Maurer, M., et al. (2018). The cryo-electron microscopy structure of huntingtin. Nature 555, 117-120.

Han, X., Ma, L., Gu, J., Wang, D., Li, J., Lou, W., Saiyin, H., and Fu, D. (2021). Basal microvilli define the metabolic capacity and lethal phenotype of pancreatic cancer. J Pathol 253, 304-314.

Hexige, S., Ardito-Abraham, C.M., Wu, Y., Wei, Y., Fang, Y., Han, X., Li, J., Zhou, P., Yi, Q., Maitra, A., et al. (2015). Identification of novel vascular projections with cellular trafficking abilities on the microvasculature of pancreatic ductal adenocarcinoma. J Pathol 236, 142-154.

Hickman, R.A., Faust, P.L., Marder, K., Yamamoto, A., and Vonsattel, J.P. (2022). The distribution and density of Huntingtin inclusions across the Huntington disease neocortex: regional correlations with Huntingtin repeat expansion independent of pathologic grade. Acta Neuropathol Commun 10, 55.

Khoshnan, A., Ko, J., and Patterson, P.H. (2002). Effects of intracellular expression of anti-huntingtin antibodies of various specificities on mutant huntingtin aggregation and toxicity. Proc Natl Acad Sci U S A 99, 1002-1007.

Klein, F.A., Zeder-Lutz, G., Cousido-Siah, A., Mitschler, A., Katz, A., Eberling, P., Mandel, J.L., Podjarny, A., and Trottier, Y. (2013). Linear and extended: a common polyglutamine conformation recognized by the three antibodies MW1, 1C2 and 3B5H10. Hum Mol Genet 22, 4215-4223.

Klumperman, J. (2011). Architecture of the mammalian Golgi. Cold Spring Harb Perspect Biol 3.

Ko, J., Ou, S., and Patterson, P.H. (2001). New anti-huntingtin monoclonal antibodies: implications for huntingtin conformation and its binding proteins. Brain Res Bull 56, 319-329.

Legleiter, J., Lotz, G.P., Miller, J., Ko, J., Ng, C., Williams, G.L., Finkbeiner, S., Patterson, P.H., and Muchowski, P.J. (2009). Monoclonal antibodies recognize distinct conformational epitopes

formed by polyglutamine in a mutant huntingtin fragment. J Biol Chem 284, 21647-21658.

Liu, Y., Chen, X., Ma, Y., Song, C., Ma, J., Chen, C., Su, J., Ma, L., and Saiyin, H. (2024). Endogenous mutant Huntingtin alters the corticogenesis via lowering Golgi recruiting ARF1 in cortical organoid. Mol Psychiatry.

Miller, J., Arrasate, M., Brooks, E., Libeu, C.P., Legleiter, J., Hatters, D., Curtis, J., Cheung, K., Krishnan, P., Mitra, S., et al. (2011). Identifying polyglutamine protein species in situ that best predict neurodegeneration. Nat Chem Biol 7, 925-934.

Nakamura, N., Rabouille, C., Watson, R., Nilsson, T., Hui, N., Slusarewicz, P., Kreis, T.E., and Warren, G. (1995). Characterization of a cis-Golgi matrix protein, GM130. J Cell Biol 131, 1715-1726.

Owens, G.E., New, D.M., West, A.P., and Bjorkman, P.J. (2015). Anti-PolyQ Antibodies Recognize a Short PolyQ Stretch in Both Normal and Mutant Huntingtin Exon 1. Journal of Molecular Biology 427, 2507-2519.

Paulson, H.L., Bonini, N.M., and Roth, K.A. (2000). Polyglutamine disease and neuronal cell death. Proc Natl Acad Sci U S A 97, 12957-12958.

Shen, M., Wang, F., Li, M., Sah, N., Stockton, M.E., Tidei, J.J., Gao, Y., Korabelnikov, T., Kannan, S., Vevea, J.D., et al. (2019). Reduced mitochondrial fusion and Huntingtin levels contribute to impaired dendritic maturation and behavioral deficits in Fmr1-mutant mice. Nat Neurosci 22, 386-400.

Tousley, A., Iuliano, M., Weisman, E., Sapp, E., Richardson, H., Vodicka, P., Alexander, J., Aronin, N., DiFiglia, M., and Kegel-Gleason, K.B. (2019). Huntingtin associates with the actin cytoskeleton and alpha-actinin isoforms to influence stimulus dependent morphology changes. PLoS One 14, e0212337.

Velier, J., Kim, M., Schwarz, C., Kim, T.W., Sapp, E., Chase, K., Aronin, N., and DiFiglia, M. (1998). Wild-type and mutant huntingtins function in vesicle trafficking in the secretory and endocytic pathways. Exp Neurol 152, 34-40.

Wang, C.E., Tydlacka, S., Orr, A.L., Yang, S.H., Graham, R.K., Hayden, M.R., Li, S., Chan, A.W., and Li, X.J. (2008). Accumulation of N-terminal mutant huntingtin in mouse and monkey models implicated as a pathogenic mechanism in Huntington's disease. Hum Mol Genet 17, 2738-2751.

Wheeler, V.C., White, J.K., Gutekunst, C.A., Vrbanac, V., Weaver, M., Li, X.J., Li, S.H., Yi, H., Vonsattel, J.P., Gusella, J.F., et al. (2000). Long glutamine tracts cause nuclear localization of a novel form of huntingtin in medium spiny striatal neurons in HdhQ92 and HdhQ111 knock-in mice. Hum Mol Genet 9, 503-513.

Wu, A.G., Wong, V.K., Xu, S.W., Chan, W.K., Ng, C.I., Liu, L., and Law, B.Y. (2013). Onjisaponin B derived from Radix Polygalae enhances autophagy and accelerates the degradation of mutant alpha-synuclein and huntingtin in PC-12 cells. Int J Mol Sci 14, 22618-22641.

https://doi.org/10.7554/eLife.111495.1.sa0